

Recently forming stalagmites from the Baradla Cave and their suitability assessment for climate–proxy relationships

Attila Demény^{1*}, Alexandra Németh¹, Zoltán Kern¹, György Czuppon¹, Mihály Molnár², Szabolcs Leél-Őssy³, Mihály Óvári⁴, József Stieber⁵

¹Institute for Geological and Geochemical Research, RCAES, Hungarian Academy of Sciences, Budapest, Hungary

²Institute for Nuclear Research, Hungarian Academy of Sciences, Debrecen, Hungary

³Department of Physical and Applied Geology, Eötvös Loránd University, Budapest, Hungary

⁴Institute of Chemistry, Eötvös Loránd University, Budapest, Hungary

⁵Stieber Environmental Ltd., Budapest, Hungary

Received: August 8, 2016; revised manuscript received: January 24, 2017; accepted: October 5, 2016

Determination of the long-term behavior of cave systems and their response to changing environmental conditions is essential for further paleoclimate analyses of cave-hosted carbonate deposits. For this purpose, four actively forming stalagmites were collected in the Baradla Cave where a three-year monitoring campaign was also conducted. Based on textural characteristics and radiocarbon analyses, the stalagmites are composed of annual laminae, whose counting was used to establish age–depth relationships. Fast and slowly growing stalagmites have different stable carbon and oxygen isotope compositions as well as trace element contents that could be attributed to differences in drip water migration pathways. The stable isotope compositions were compared with meteorological data of the last ~100 years indicating that carbon isotope compositions of the stalagmites may reflect changes in precipitation amount, while oxygen isotope compositions are more related to temperature variations. The combined textural–geochemical–meteorological interpretation lead us to select the isotope record that can best reflect variations in environmental conditions and can be used for further evaluation of the climate–proxy relationships.

Keywords: speleothem, stable isotope compositions, actively forming stalagmites, Baradla Cave, temperature, precipitation amount

*Corresponding author: Attila Demény; Institute for Geological and Geochemical Research, RCAES, Hungarian Academy of Sciences, Budaörsi út 45, H-1112 Budapest, Hungary
E-mail: demeny@geochem.hu

This is an open-access article distributed under the terms of the Creative Commons Attribution License, which permits unrestricted use, distribution, and reproduction in any medium for non-commercial purposes, provided the original author and source are credited.

Introduction

It is widely known that geochemical analyses of speleothem formations provide valuable climate proxy data for paleoclimate evaluation and >100 articles were published every year in the last decade dealing with studies based on speleothem research. Firm interpretation of the proxy data requires knowledge of the climate–proxy relationship, i.e., how the speleothem compositions reflect environmental parameters, such as precipitation amount, its seasonal variation, temperature changes, vegetation, and soil biological activity. A widely accepted method to establish a proxy–environment transfer function is cave monitoring when physical and chemical parameters are monitored outside and inside the cave in order to determine the driving factors of carbonate precipitation and variations in carbonate geochemistry (Genty 2008; Matthey et al. 2008, 2016; Boch et al. 2011; Riechelmann et al. 2011; Baker et al. 2014; Meyer et al. 2014; Osácar et al. 2014; Van Rampelbergh et al. 2014; Casteel and Banner 2015; Pu et al. 2015, 2016; Treble et al. 2015; Duan et al. 2016) or even to link drip water and carbonate compositions to operations of meteorological systems (Moreno et al. 2014; Mischel et al. 2015; Moquet et al. 2016). The main problems with cave monitoring are that many caves are severely protected with restricted access and monitoring activities seldom reach the length of 10 years period (Fairchild and Baker 2012; Matthey et al. 2016). Monitoring for some years can provide essential information on the cave’s operation at present; however, its long-term behavior is difficult to judge from the limited length of time series data. An alternative approach is analysis of actively growing stalagmites that also cover the last decades or centuries and whose geochemical proxies can be directly compared with instrumental meteorological data (e.g., Baker et al. 2007; Matthey et al. 2008; Boch and Spötl 2011; Orland et al. 2014; Van Rampelbergh et al. 2015). The bottleneck in this case is the age–depth relationships, i.e., precise dating of the geochemical data. Layer counting of laminated deposits is the most accurate method provided that the ages of a part of the laminae can be anchored by independent evidence. Such evidence can be known dates of starting deposition and collection, continuous deposition of layers whose annual formation is proven, event marker horizons like ^{14}C bomb peak, or any well-known environmental change like a volcanic eruption whose signal can be detected. Radiocarbon analysis is a powerful method as it may detect the presence of the 1964–1965 bomb peak in the carbonate deposit, proving the annual nature of lamina formation (simply by counting laminae between the presently active surface and the bomb peak) and fixing the anchor date of 1964–1965 (e.g., Genty and Massault 1999; Matthey et al. 2008; Rudzka-Phillips et al. 2013). Having established age–depth relationship, speleothems are frequently studied by means of trace element and stable isotope analyses (the latter expressed as δD , $\delta^{13}\text{C}$, and $\delta^{18}\text{O}$ values – with abbreviations of “w” for water and “carb” for carbonate – see the Analytical methods section).

Stable carbon and oxygen isotope compositions of speleothem carbonates depend on numerous factors that make the interpretation of isotope values as climate proxies rather difficult. Fairchild and Baker (2012) have compiled recent knowledge on speleothem research in an extensive review, in which the possible factors governing

$\delta^{13}\text{C}$ and $\delta^{18}\text{O}_{\text{carb}}$ values are thoroughly investigated. Due to the large number of related papers, the reader is advised to see their review of the scientific literature. The carbon isotope compositions are determined or influenced by the type of vegetation above the cave (relative proportions of C3 and C4 plants), the efficiency of biological activity in the soil (regulating the amount of biogenic, ^{13}C -depleted CO_2 dissolved in the groundwater), the degree of carbonate rock dissolution, the carbonate precipitation in the rock's voids due to evaporation during percolation ("prior calcite precipitation"), and kinetic fractionation due to CO_2 degassing. Variations in drip rate can have a further influence as lower drip rates mean longer solution residence time on the stalagmite surface and higher degree of degassing, evaporation, and isotope exchange with the ambient atmosphere (Scholz et al. 2009; Boch et al. 2011).

Although the oxygen isotopic composition of the precipitating carbonate is mainly determined by the water composition and the formation temperature, kinetic fractionation due to fast precipitation (Dietzel et al. 2009) and H_2O evaporation on the speleothem surface (in case of strong ventilation) can also have strong influences. CO_2 degassing and H_2O evaporation induced by enhanced ventilation results in positive $\delta^{18}\text{O}-\delta^{13}\text{C}$ correlation moving from the axis to the stalagmite flanks due to kinetic fractionation processes (Hendy 1971; Mickler et al. 2006). This effect may be detected by analyzing the carbonate's C and O isotope compositions along single growth layer ("lamina"), called Hendy-test after the seminal paper of Hendy (1971). Kinetic fractionation-related isotope variations (e.g., Mickler et al. 2006) may exceed the fluctuations induced by environmental changes and can obscure the primary climate-related proxy signal; therefore, stalagmites formed in ventilated caves are generally avoided during paleoclimate research and the Hendy-test is used as a selection tool. However, since the isotope compositions are usually measured in the axes of stalagmites (i.e., at the same position with the same degassing rate), the detection of kinetic fractionation in growth laminae does not necessarily mean that the stalagmite is not suitable for paleoclimate analysis, provided that the ventilation degree did not fluctuate in time. The evaluation is complicated by the fact that not only ventilation-related kinetic fractionation, but changes in climate parameters (temperature and humidity at the surface above the cave) can also produce coupled $\delta^{13}\text{C}$ and $\delta^{18}\text{O}$ shifts in the carbonate (Dorale and Liu 2009). To overcome these problems, those isotope records are considered as most suitable for paleoclimate/environmental analyses that can be replicated in several stalagmites (Replication Test, Dorale and Liu 2009).

The oxygen isotope signature in the precipitated carbonate is mainly determined by two factors. The first factor is the cave temperature at the time of calcite formation and the second factor is the isotopic signature of the drip water. The experimentally determined effect on the calcite isotopic composition through the temperature dependence of calcite-water isotope fractionation is $-0.24\text{‰ } ^\circ\text{C}^{-1}$ in the range of $5\text{--}20\text{ }^\circ\text{C}$ for equilibrium precipitation (O'Neil et al. 1969). The oxygen isotope composition of the drip water from which the carbonate is precipitated is determined mainly by the composition of meteoric water above the cave, although further processes can modify the composition of the infiltrating water. The water percolating

in the karstic system may undergo evaporation (causing ^{18}O -enrichment) from the soil zone to the stalagmite surface. Mixing of waters deriving from different reservoirs (e.g., slowly migrating water stored in rock voids and rapidly moving water in open fractures) may also affect the final composition of the drip water arriving at the stalagmite surface. The final drip water composition produced by these processes and the formation temperature will collectively determine the oxygen isotope value of the precipitating carbonate (O'Neil et al. 1969).

Another form of temperature effect is the relationship between atmospheric temperature and the oxygen isotope compositions of precipitation water (Dansgaard 1964). Using the extensive $\delta^{18}\text{O}$ data set of global precipitation water collected at the IAEA/WMO stations, Rozanski et al. (1993) established an average of $0.58\text{‰ }^{\circ}\text{C}^{-1}$ for the $0\text{--}20\text{ }^{\circ}\text{C}$ range. Since this relationship can change locally depending on the distance from the moisture source and on altitude (e.g., Salamalikis et al. 2016), the best approach is to determine the site-specific value by monitoring atmospheric temperature and precipitation water composition. Assuming that the seasonal distribution of precipitation changes, the dominance of winter vs. summer precipitation in the infiltrating water can vary, causing additional variation in the drip water composition and in the calcite. The oxygen isotope composition of the precipitation may also change, depending on the source region and the fractionations due to rainout and evaporation (e.g., Lachniet 2009).

Many of these processes are competitive, in the sense that they may induce isotopic shifts in opposite directions, making the interpretation of stable isotope compositions as climate proxies difficult even for those speleothems that were formed in the last century and whose compositions can be compared with meteorological data (e.g., Baker et al. 2008; Van Rampelbergh et al. 2015). Nevertheless, in most cases only some factors dominate, whereas others just modulate the isotopic compositions (Van Rampelbergh et al. 2014).

The aim of this study was to collect and analyze actively forming stalagmites from the Baradla Cave, where numerous stalagmites have been and will be used for paleoclimate research, and determine the relationships between their geochemical proxy data and environmental parameters. Four actively growing stalagmites were collected from the Baradla Cave and studied by means of optical microscopy, radiocarbon, stable isotope, and trace element analyses. The geochemical data are correlated in the stalagmites and compared with meteorological data, and finally a composite isotope record is selected for further analyses.

The Baradla Cave and the studied stalagmites

The Baradla Cave is situated in north-east Hungary ($\text{N}48^{\circ}28' \text{E}020^{\circ}30'$) at the Hungarian–Slovakian border (Fig. 1), beneath a forested area with a mean elevation of 300–450 m a.s.l. The system was formed in lagoon facies of the Wetterstein Limestone of the Triassic (Ladinian) age and is characterized by almost horizontal passages. The area is under the influence of European cyclone tracks with the most important

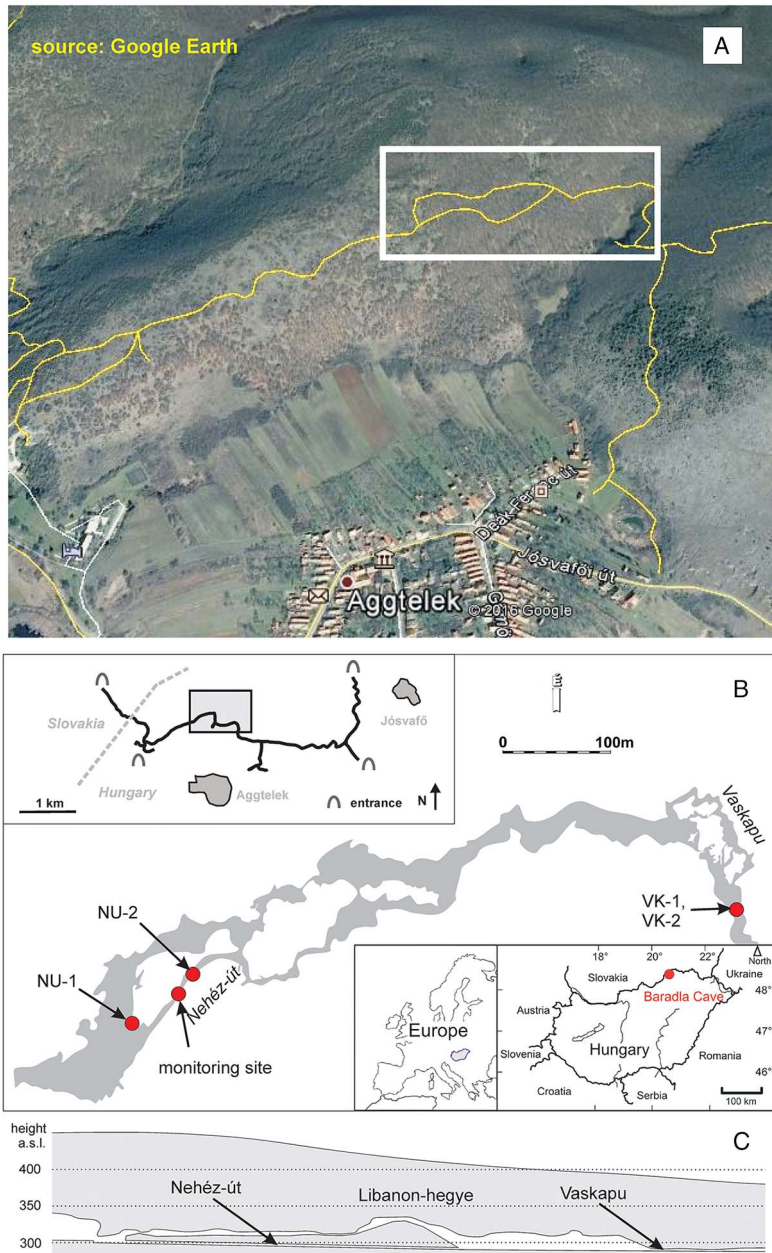


Fig. 1

A: Position of the studied part of the Baradla Cave (yellow line) shown in a satellite image (source: Google Earth). B: Location and map of the Baradla Cave system (source: Aggtelek National Park). Gray shaded area shows the place of the detailed map. Positions of sampling sites at the Nehéz-út and Vaskapu branches are shown. C: Vertical cross section of the Nehéz-út and Vaskapu section of the Baradla Cave

cyclogenesis centers in the Icelandic and the Western Mediterranean regions (Bartholy et al. 2006, 2009). Cyclones starting-up near these regions transport marine moisture to Hungary (Bottyán et al. 2013; Czuppon et al. 2015) by the induced frontal systems. Most Icelandic cyclones arrive in winter, but approximately 30 cyclones derive from the Mediterranean area, most frequently in spring (Kelemen et al. 2015) and autumn (Bottyán et al. 2013; Czuppon et al. 2015). Significant weather influences could also come from the East and North (Bartholy et al. 2006). However, this weather pattern brings cold/dry air into the region, so precipitation is typically not accompanied with these macrocirculation situations. The most characteristic season and situation when such influences can be prevailing is winter when cold polar/continental air masses intrude to the region. Monthly averages of precipitation amount, temperature, and potential evapotranspiration data of the CARPATCLIM database (Fig. 2; Szalai et al. 2013) indicate that infiltration may occur in the period of in the cold months (~October to April), while evapotranspiration exceeds precipitation in the warm months.

Actively forming stalagmites were collected at two sites, the Nehéz-út and the Vaskapu branches within about 1 km from the nearest entrance (Fig. 1). The Nehéz-út branch is situated mainly below a hill (Fig. 1A) with a rock cover reaching 150 m thickness, whereas the Vaskapu branch is under a valley with a rock cover thickness of about 100 m (Fig. 1C). Monitoring of physicochemical parameters (temperature, drip water pH, conductivity, and cave air CO₂ concentration) and isotope compositions of drip water in the Baradla (Fig. 1) and the nearby (~3 km) Béke Caves, as well as the amount and isotope compositions of precipitation water collected at Jósmafő (~5 km to the east from the cave site, Fig. 1) was conducted in the period between 2013 and 2016. The entire data set will be published in a companion paper (Czuppon et al., submitted), here we summarize the observations relevant to this study. Descriptions of analytical instruments are given in the

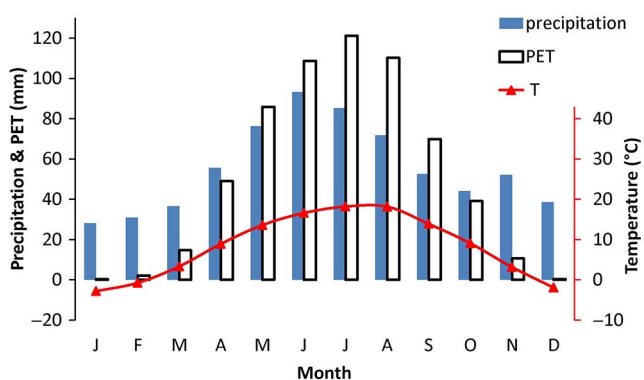


Fig. 2
Monthly averages of precipitation amount, potential evapotranspiration (PET), and atmospheric temperature (from 1961 to 2010) at the Baradla Cave based on the CARPATCLIM database (Szalai et al. 2013)

Analytical methods section. Cave temperature was 9.7 ± 0.5 °C, CO₂ content was $3,500 \pm 1,100$ ppm, and pH was 7.9 ± 0.3 ($n = 14$). Within this monitoring campaign, the isotopic compositions of 30 precipitation water samples were compared with 19 drip water samples collected at the Nehéz-út site within the Baradla Cave. The δD and $\delta^{18}O$ values of precipitation range from -110.0‰ to -19.5‰ and from -15.5‰ to -3.0‰ , respectively. Both isotope compositions show seasonal fluctuations with high values in summer and low values in winter (Fig. 3). The Local Meteoric Water Line is given by the equation $\delta D = 7.4 \cdot \delta^{18}O + 5.2$ for the monthly average data. The annual amount weighted mean δD and $\delta^{18}O$ values of precipitation are -62.7‰ and -9.1‰ , respectively. The isotopic compositions of drip waters show almost constant values ($\delta D \sim -64.7 \pm 1.9\text{‰}$ and $\delta^{18}O \sim -9.4 \pm 0.3\text{‰}$) for the studied period (Fig. 3). Although a slight season-related fluctuation appears in the data, the variations are close to the analytical precision, hence these are not significant. The average values are more negative than the annual average of amount weighted precipitation compositions, suggesting more contribution from cold season precipitation (Supplementary Table S1). The contribution of cold seasons' precipitation can be calculated by mass balance calculation using the amount weighted average isotopic compositions of warm (April to September) and cold (October to March) seasons (Supplementary Table S1), that yielded a cold season contribution of 90%.

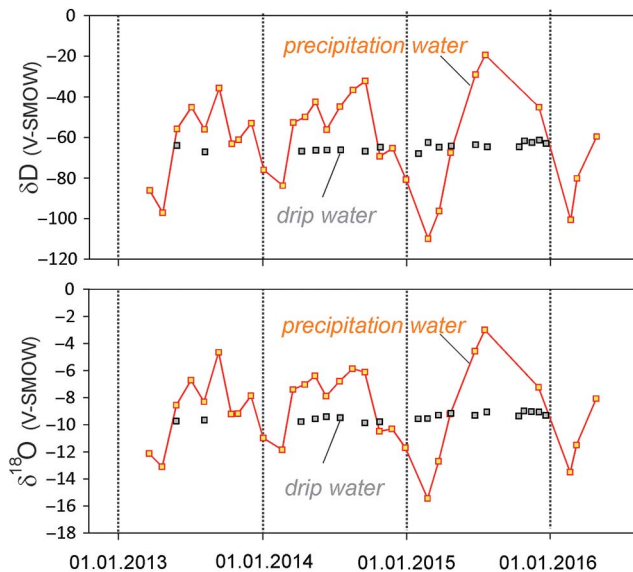


Fig. 3
Stable H and O isotope compositions (in ‰) of precipitation water collected at Jósvalfő and drip water of the Nehéz-út site

Using monthly averages of atmospheric temperature and meteoric water composition, the analyses yielded a temperature dependence of $0.30\text{‰ }^{\circ}\text{C}^{-1}$ in accordance with earlier results from the central area of the Pannonian Basin (Deák 1995 cited in Fórizs 2003; Vodila et al. 2011) and in the northern part of the Carpathians (Holko et al. 2012). Combining the temperature effects on carbonate–water oxygen isotope fractionation and meteoric water composition, the net effect of temperature change is found to be $0.06\text{‰ }^{\circ}\text{C}^{-1}$ for the area of Baradla Cave, consequently the carbonate composition would only slightly follow the oxygen isotope change in the infiltrating rainwater.

Four actively forming stalagmites were collected from the Baradla Cave at the Nehéz-út (“NU”) and the Vaskapu (“VK”) branches (Fig. 1B). The stalagmites’ locations were well above any flood level observed before. All the stalagmites are composed of calcite on the basis of control X-ray diffraction and infrared spectroscopic analyses. Since there was no mineralogical variation in the stalagmites, these analyses were only used as tests and will not be discussed in this paper. Stalagmite NU-1 (collected in May 2013) is an ~5 cm high, irregular “hump” with a central depression where the dripping water impinged from a height of ~3.5 m. Its cross section shows fine, but rather irregular lamination and a strongly porous structure (Fig. 4A) especially in the central part. Sample NU-2 (collected in June 2014) is an isometric, rounded stalagmite formed from drip water arriving from ~1.5 m height. It shows fine lamination and compact structure in cross section (Fig. 4B). The macroscopic textures show internal variation within the stalagmite. At the bottom part (~5 to 7 cm from the top), the stalagmite is composed of clear, lamination-free calcite that turns into a white, laminated calcite upward. At ~1.5 cm from the top, there is again a sudden structural change where the formation axis seems to be shifted. Samples from the Vaskapu site (VK-1 and VK-2) were collected in April 2015. The stalagmites were deposited on a cave surface that was most probably created during construction work in 1925 when a bridge was built close to the site (Székely 2014). Both stalagmites were formed on a clay deposit with the drip water arriving from ~1.5 m height. Sample VK-1 is ~5 cm high with a compact texture and fine lamination visible in cross section (Fig. 4C). Sample VK-2 reaches 7 cm in height (Fig. 4D), the internal texture is rather porous similarly to sample NU-1. All of the four stalagmites consist of opaque white and translucent gray laminae; however, the opaque white texture is more abundant in VK-1, NU-1, and VK-2 stalagmites than in NU-2. Opaque white laminae tend to increase in thickness where they drape over the older parts of the stalagmite.

Analytical methods

Cave air and water temperatures were determined using a *GMH-3710* type Pt-100 digital thermometer (range from -199.99 to $+199.99$ °C, resolution: 0.01 °C, precision: ± 0.03 °C). CO₂ concentration in cave air at 150 cm from the ground was

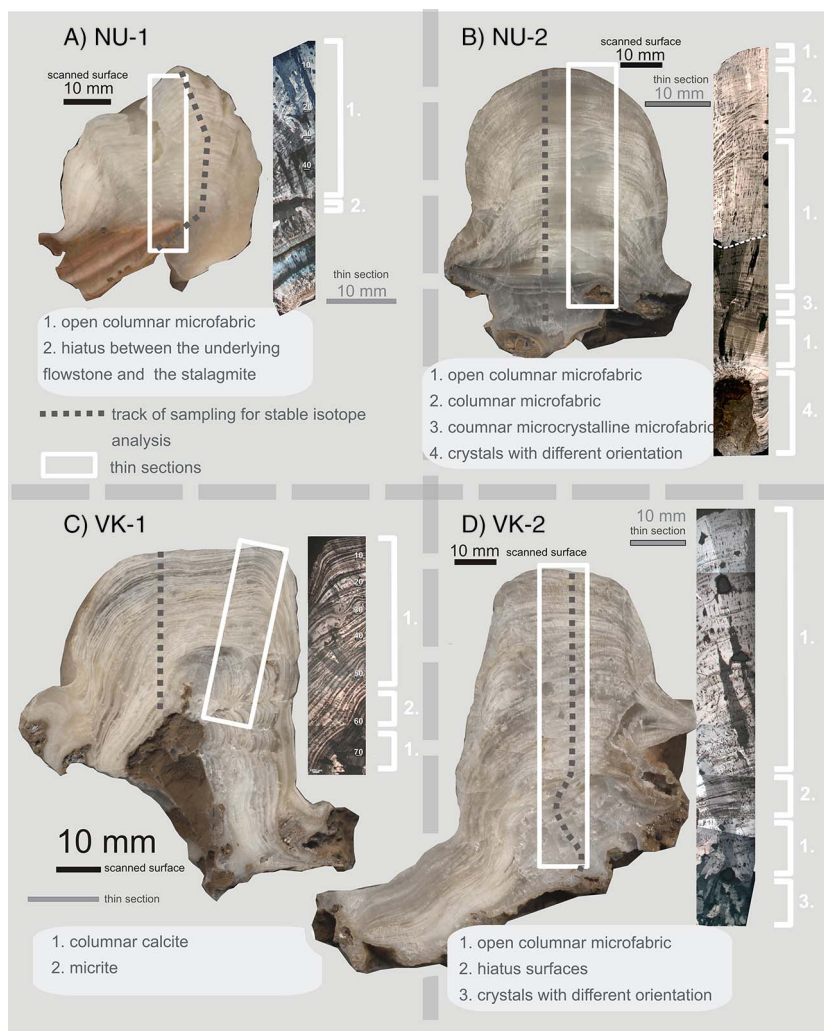


Fig. 4 Polished surfaces of cross sections and photomicrographs taken (using crossed nicols) along the growth axis of each stalagmite with their micrologs, based on Frisia (2015). The thin sections were prepared from the opposite surfaces to the scanned ones; therefore, they are in a reflected position. Sampling tracks for stable isotope analyses of the studied stalagmites are shown as dashed lines

measured using different NDIR instruments for low (*TESTO-535*, range 0–10,000 ppm, resolution: 1 ppm) and high (*ANALOX ASPIDA*, range 0–10 vol. %, resolution: 0.01 vol. %) levels. Electrical conductivity and pH values of drip water samples were measured using a *COMBO PH & EC* instrument (EC range 0–3,999 $\mu\text{S}/\text{cm}$,

resolution: 1 $\mu\text{S}/\text{cm}$, pH range: 0.00–14.00, resolution: 0.01) with precisions of 2% and 0.05, respectively. Optical microscopic analyses were done in crossed-polarized transmission light using a Nikon Eclipse E600 POL optical microscope on polished thin ($\sim 100\ \mu\text{m}$) sections. Sample preparation for accelerator mass spectrometry analyses were conducted following standard procedures (Molnár et al. 2013a), the $^{14}\text{C}/^{12}\text{C}$ and $^{13}\text{C}/^{12}\text{C}$ ratios were measured by the Environ MICADAS ^{14}C facility in the Hertelendi Laboratory of Environmental Studies in Debrecen, Hungary (Molnár et al. 2013b). Overall measurement uncertainty for a modern sample is $<3\%$, including normalization, background subtraction, and counting statistics. Activities are expressed in percent modern carbon (pMC).

Stable carbon and oxygen isotope compositions were determined on calcite powder drilled at a spatial resolution of 0.6–1 mm using a Thermo Finnigan delta plus XP continuous flow isotope ratio mass spectrometer equipped with a Gasbench II automated sample preparation device at the Institute for Geological and Geochemical Research (IGGR), Budapest (following the analytical procedures of Spötl and Vennemann 2003). Isotopic compositions are expressed as $\delta^{13}\text{C}$ and $\delta^{18}\text{O}$ in ‰ relative to V-PDB, with a precision is better than $\pm 0.1\%$, as based on replicate analyses of samples and international standards (NBS-18, NBS-19, and LSVEC) supplied by the International Atomic Energy Agency.

Trace element concentration measurements were conducted at the Institute of Chemistry, Eötvös Loránd University. About 10 mg of powdered sample was weighed into high purity 15 mL polypropylene centrifuge vials using an ultra-micro balance, then dissolved in 12 mL, $0.5\ \text{mol dm}^{-3}$ nitric acid (Suprapure grade, E. Merck, Darmstadt, Germany). For the quantification $120\ \mu\text{L}$, $1\ \text{mg dm}^{-3}$ In internal standard solution was added. The analysis was carried out using an Element 2 inductively coupled plasma sector field mass spectrometer (Thermo-Finnigan, Bremen, Germany). External calibration and internal standard solutions were prepared from multi- and single-element ICP standard stock solutions (E. Merck, Darmstadt, Germany).

For meteorological data, gridded climate data were used in this study in order to avoid data gaps and inhomogeneities of single station records. CARPATCLIM is a recently released regional climate database (time span: 1961–2010, grid space: 0.1°) derived from carefully homogenized station records (Szalai et al. 2013) providing high-quality and accurate meteorological data for the Carpathian region over the past 50 years with exceptionally high spatial resolution. In order to expand the time span of the proxy–climate comparison updated global gridded climate data set (CRU TS3.23) from monthly observations at WMO meteorological stations across the world (Harris et al. 2014) were also utilized (time span: 1901–2014, grid space: 0.5°). However, this global data set has a much coarser spatial resolution. Monthly mean temperature and precipitation totals were extracted for the grid cells covering the Baradla site from both data sets, then annual and seasonal (three-month averages) averages were calculated.

Results and discussions

The results of lamina counting, thickness measurements, radiocarbon, stable isotope, and trace element analyses are listed in Supplementary Tables S2–S6 for the studied stalagmites and for the host rocks collected in the Baradla Cave (see Supplementary Material).

Petrographic analyses

As a general observation, macroscopical features described above are related to microfabric changes. Macroscopically similar parts, however, are revealed to contain several different microfabrics (Fig. 5). Observed under cross-polarized light the macroscopically opaque and white parts of the stalagmite can have columnar open, columnar microcrystalline, dendritic, and micritic microfabrics (Frisia 2015). Columnar open texture (Fig. 5A, B, D, E, and J) is made of slightly elongated calcite crystals showing columnar extinction pattern under crossed polars. The intercrystal porosity is high in this texture; pores are appearing along the lamination (Boch et al. 2011). Columnar microcrystalline (Genty et al. 1997) is a similar texture (Fig. 5D), it can be recognized by the very irregular composite crystal boundaries (Fig. 4B). The extinction domains of these crystals sometimes interfingered as they often grow with different orientation. Dendritic fabric consists of branching polycrystals and it has also high intercrystalline porosity (McDermott et al. 1999; Fig. 5A and B). Dark laminae of micrite were observed abundantly in the macroscopically opaque and white laminae of the VK-1 stalagmite (Fig. 5I). This microfabric contains smaller crystals (<2 µm; Frisia 2015) and UV fluorescent organic material, and it is likely to be replaced by sparitic crystals during diagenesis. Macroscopically clear, light gray parts were observed to be compact columnar calcite (Frisia et al. 2000). This low-porosity microfabric is made of columnar calcite crystals with straight extinction boundaries. These microfabrics vary along the axis of each stalagmite, but they can also grade into each other laterally along the same laminae.

The *NU-1 stalagmite* is characterized by high porosity and relatively thick lamination. The former is partially due to its microfabric (columnar open and dendritic calcite) and to a great number of dissolution vugs between the elongated crystals. This stalagmite started to grow on a piece of flowstone: at ~23 mm from the top of the thin section, a sharp surface can be observed, where termination of calcite crystals was covered by clayey material (Fig. 5C). This is the onset of the stalagmite's formation. The samples for geochemical analysis were drilled along a longer track (Fig. 4, dashed line). Here the lowermost 12 drills sampled the flowstone and the non-laminated part of the stalagmite. The first drill which sampled the laminated material was at 36 mm depth, measured along the track. The NU-1 stalagmite consists of entirely columnar open and dendritic microfabric. The former fabric is more typical along the growth axis. Each column with the same extinction can be followed along the growth axis;

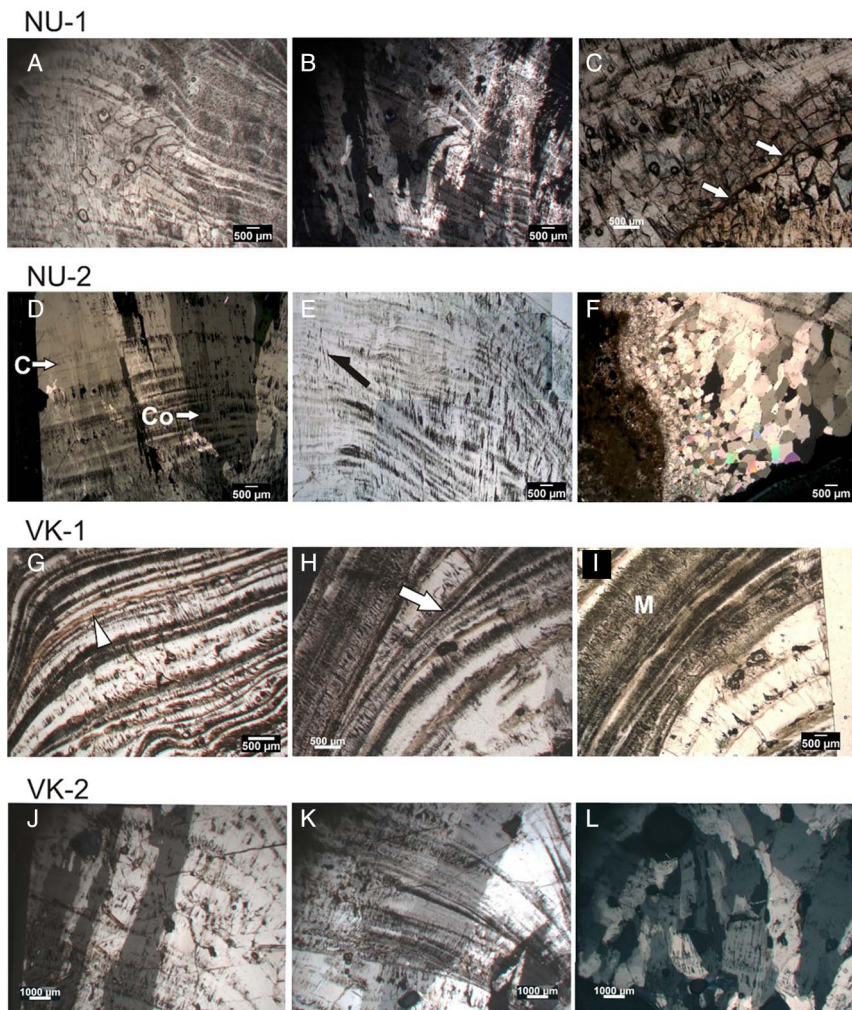


Fig. 5

A: 1N photomicrograph of the upper 20 mm of the NU-1 stalagmite. B: The same with 2N. Note the gradual transition between the open columnar (Co) and the dendritic (D) microfabrics (from left to right). C: Hiatus surface aligned by white arrows at the basis of the stalagmite. D: Columnar calcite microfabrics in the axial part of NU-2 stalagmite grading into open columnar microfabric, 2N photomicrograph. E: Gradual transition between a more compact and a more porous columnar microfabric from the axis to the side of the stalagmite (left to right). The black arrow indicates a surface where the microstratigraphical stacking changes to progradational. 1N photomicrograph. F: Calcite with different orientation and high birefringence color observed at the bottom of the stalagmite. G: Columnar calcite microfabric in the VK-1 stalagmite, 2N photomicrograph. The white triangle indicates a series of upward-thinning laminae. H: Lateral truncation of laminae on the side of the stalagmite. I: Micritic laminae (M) with very reduced lamina thickness, 1N photomicrograph. J: Open columnar calcite microfabrics in the VK-1 stalagmite, 2N photomicrograph. K: Dark, erosion surfaces cutting into each other in the lower part of the stalagmite. L: Calcite with different orientation and no lamination observed at the bottom of the stalagmite

however, they become shorter with uneven boundaries toward the side of the stalagmite. Here, a gradual transition to dendritic fabric can be observed (Figs 4A, 5A, and 5B).

Lamination in both microfabrics is composed of porous and compact sub-laminae. The porous sub-laminae are UV fluorescent and they tend to thicken toward the sides. The columnar open microfabric and thick lamination in the axial position suggest relatively high and constant drip rate and continuous deposition. Columnar open microfabric was observed to form at near equilibrium conditions and at low supersaturation (Frisia et al. 2000). This open microfabric was also associated with relatively high Mg/Ca ratio, which can be explained by late-diagenetic dissolution of dolomite host rock. While Frisia (2015) suggested that dendritic fabric may indicate variable drip rates and supersaturation degree, in the NU-1 stalagmite the formation of dendritic fabric can be explained by its marginal position, where carbonate precipitates from droplets derived from splashing. Considering that the source of dripping water was situated high above the stalagmite (3.5 m) and that the stalagmite has an irregular shape with a central depression (“splashing cup,” Curl 1973), the dendritic fabric may be related to the splash effect associated with rapid degassing. The high porosity and the dissolution vugs suggest that this stalagmite would not be an ideal sample for palaeoclimatic reconstruction.

The NU-2 stalagmite is characterized by a more compact texture, and several different microfabrics can be observed along its growth axis. This stalagmite started to grow on a silty substratum. While the lowermost part (under 54 mm from the top of the sample) is also calcite, it has strikingly different petrographical features. The macroscopically clear calcite here is made of two different types of crystals. The first type is a collection of small crystals which grew in isopachous geometry on the surface of the substratum probably under phreatic conditions, in a small pool. They are covered by larger crystals with patchy extinction pattern and high birefringence color. There is a gradual transition between this type of crystals and the columnar crystals that form the rest of the stalagmite. As the birefringence color changes to gray, the crystals have a more elongated shape and lamination begins. This shift can be explained by the different orientation of the calcite crystals below 54 mm compared with the rest of the columnar crystals in the stalagmite.

The first laminae between 48 and 54 mm are thick and not parallel to each other (Figs 4B and 5F). From 48 to 43 mm, lamination (alternating porous and compact sub-laminae) is thin and parallel in the columnar calcite. Between 39 and 43 mm from the top of the sample, there is a relatively porous part of the sample, where columns of uniform extinction terminate. Here, pores are not parallel to the growth axis as well as the orientation of the columnar crystals, which have very uneven extinction boundaries. This part of the sample can be described as columnar microcrystalline microfabric. Between 39 and 12.5 mm and between 0 and 3.5 mm from the top of the stalagmite, open columnar microfabric is dominant along the axis, with thick porous sub-laminae in the couplets. Between 3.5 and 12.5 mm, however, the axis consists of low-porosity columnar calcite. It grades into open columnar calcite as porous sub-

laminae thicken toward the sides (Fig. 5E). Lamination is thinner here than the rest of the sample. Between 3.5 and 12.5 mm, the stacking pattern of the laminae is retractionsal: they do not cover the entire surface of the underlying laminae but tend to thin out, while under 12.5 mm the microstratigraphic stacking pattern is progradational.

The alternation between the more compact and the more open columnar microfabrics coincides with the layer-bounding surfaces. Open columnar fabric with relatively thick porous sub-laminae, therefore, can be connected to the progradational growth of the stalagmite, while the occurrence of columnar microfabric between 3.5 and 12.5 mm can be connected to a retractionsal pattern. The shift from progradational to retractionsal microstratigraphic stacking patterns was interpreted as decreasing drip rates by Muñoz-García et al. (2016). In accordance, open columnar microfabric was observed to form under high discharge variability by Boch et al. (2011) and interpreted as an indicator of higher drip rate by Frisia (2015), while columnar microfabric was associated with regular drip rates and low supersaturation by Frisia et al. (2000). The formation of the NU-2 stalagmite, therefore, was clearly affected by changing drip rates. The surfaces between the different microfabrics do not have detrital coating or any sign of erosion, therefore, probably the formation of the stalagmite was continuous.

The *VK-1 stalagmite* is generally characterized by a macroscopically white, compact texture which was revealed to be mostly columnar calcite. At 22 mm depth, however, the compact sub-laminae disappear completely and a 2.9-mm thick, densely laminated micritic band can be observed, even macroscopically (Figs 4C and 5I). Along the bands, micrite was partially recrystallized into microsparite.

The lamination in this stalagmite is quite different compared to the other three samples: each lamina couplet consists of a thin, dark, micritic sub-lamina and a thicker compact sub-lamina, which has a sharp upper surface. The shape of calcite crystallines growing out from the micritic sub-laminae is distorted, resulting crooked pores (Fig. 5G and H). Micritic sub-laminae occasionally became thicker along the growth axis (the most striking ones are at 8.6, 4.6, and 2 mm depth from the surface of the stalagmite). At ~12 mm depth, there is a sharp change in the lamination. Below this depth, the lamination is easily followed toward the sides, whereas between ~12 and 8.6 mm, the deposition is laterally uneven (Fig. 5G and H).

While the *VK-1 stalagmite* has a symmetric shape, the axis of growth however changes occasionally. Lateral thinning of laminae as a retractionsal microstratigraphical stacking pattern can also be observed at several places in the stalagmite (Figs 4C and 5H). Under the overlapping surfaces of the next stack of laminae with progradational pattern, a series of upward-thinning laminae can be observed (Fig. 5G, white triangle). Columnar calcite is the indicator of relatively low but constant drip rates (Frisia 2015). On the other hand, the *VK-1 stalagmite* shows several upward-thinning series of lamination and surfaces of selective deposition that can be associated with gradually decreasing drip rates from time to time. The dual nature of the lamination (alternating dense columnar calcite and micrite sub-laminae) suggests strong seasonal dispersion in the drip rates or in their impurity

content. The densely laminated, micritic band in the lower part of the stalagmite may have formed during a time period with extremely low drip rates and/or biomediation (Frisia et al. 2012; Frisia 2015). It is possible, that around this time, carbonate precipitation ceased for an unknown number of years which makes the dating of the lower part of the stalagmite problematic by lamina counting. Based on these observations, we consider the VK-1 sample a slowly forming stalagmite, strongly constrained by the seasonal changes in drip rates.

The porous VK-2 stalagmite consists mostly of open columnar fabric (Fig. 5J). From 55 mm from the top to the basis of the stalagmite, a similar microfabric can be observed as in the lowest part of the NU-2 sample. Presumably columnar calcite crystals can be observed with varying orientation and no lamination (Fig. 5L). Between 44 and 55 mm, several dark layers appear (Fig. 5K). These distinct erosional surfaces are cutting into one another and they are also not parallel with the lamination above them. This part can be considered to contain a number of hiatuses with an unknown temporal resolution. The microfabric between 44 mm and the top of the sample is open columnar calcite. Lamination could be recognized in this part of the stalagmite; however, laminae are not as well defined as in the other three stalagmites. Similarly to the NU-1 and NU-2 samples, laminae consist a more porous and a more compact sub-laminae. Lamina thickness and porosity – similarly to NU-1 – is relatively high and detrital laminae are missing. Based on these observations and its typical open columnar microfabric, we consider this stalagmite (except its lowest part) a continuously and rapidly growing form.

Petrographic analysis of the four stalagmites revealed that their lamination may not have been caused by the same process. In the VK-2, NU-1, and NU-2 stalagmites, it was probably originated from the changing supersaturation levels, as more compact and more porous sub-laminae alternated. The supersaturation of the drip water depends on largely the $p\text{CO}_2$ of the cave air, which is high in summer and low in winter in the Baradla Cave. While we could not prove the seasonality of these sub-laminae by monitoring carbonate precipitation, several studies (Mattey et al. 2008) already observed similar, seasonally forming lamina couplets in recent stalagmites, affected by the changing $p\text{CO}_2$ level of the cave atmosphere. In the VK-1 stalagmite, decreasing drip rate/biomediation could form the bright fluorescent micritic sub-laminae. Without a long enough monitoring data series, the seasonal origin of these laminae cannot be proved; however, we tried to test their annual origin by comparing the results of lamina counting and radiocarbon dating.

Speleothem dating by lamina counting and radiocarbon analyses

On the basis of published analogs (Baker et al. 2008; Mattey et al. 2008; Boch et al. 2011) and preliminary ^{14}C data, couplets of macroscopically dark and white laminae in the NU-1 and NU-2 stalagmites were interpreted as annual layers (Demény et al. 2016), hence lamina counting offers a direct approach to establish a timescale for the derived geochemical proxy records. Counting annual laminae from the surface that

represents the date of collection, the years of formation can be assigned to the individual layers, provided that (1) every annual layer is detected, (2) sub-annual layers are not determined as annual laminae, and (3) no hiatus occurred during the stalagmite formation.

Lamina counting was performed along the growth axis of the stalagmites. The thickness of laminae was also measured: we determined lamina thickness as the distance between the sharp upper surface of a compact sub-lamina and the lower boundary of the underlying porous sub-lamina. The raw lamina counting yielded the following periods of deposition: NU-1: 47 years, NU-2: 154 years, VK-1: 72 years, VK-2: 88 years, although it is important to note that the bottom parts (the oldest ~1 cm) of the stalagmites are weakly or not laminated and consequently lamina counting could not be conducted. Using the lamina counting dates, radiocarbon activities (as pMC values) were plotted as a function of time in Fig. 6.

It is apparent that all of the stalagmites yielded different radiocarbon activity patterns. Interestingly, the four stalagmites from the same cave display radiocarbon patterns characteristic for different regions of Europe, where the ^{14}C patterns were used as a karstic environment classification tool (Rudzka-Phillips et al. 2013). The “bomb peak” of 1964–1965 is best expressed in NU-2, although with strong fluctuations in the youngest part, a slight shift of the pMC maximum from the bomb peak, and a significant activity drop at the older part (at 27 mm from the top, Fig. 7). At around 1960 (raw lamina age), two radiocarbon sampling spots are partly overlapping resulting in an unrealistically steep ^{14}C rise. This is the part where a sudden structural change is observed, hence a hiatus may be assumed. NU-1 shows an almost constant radiocarbon activity, although with slightly elevated pMC values after the bomb peak. The pattern of VK-1 is completely different from those showing signs of the bomb peak, whose lack in VK-1 might be related to a hiatus. Finally, stalagmite VK-2 shows a clear sign of the bomb peak with about 3 years delay, although the pMC values are lowest in this sample. As a next step, all of the data and patterns were compared with textural characteristics.

A possible indicator of textural change is lamina thickness, as decreased thickness means reduced deposition rate as consequence of drip rate and drip water chemistry changes. The radiocarbon patterns of the NU-1 and VK-2 stalagmites have no clear relationships with the lamina thickness values. The NU-2 and VK-1 stalagmites display macroscopically detectable textural changes that might indicate hiatuses (arrows 1 and 3 in Fig. 7). The very strong ^{14}C activity drop in NU-2 at about 27 mm from top is associated with a significant reduction in deposition rate that can be attributed to reduced drip rate. As a consequence, increased CO_2 degassing may have removed dissolved CO_2 that carried modern C, enriching the concentration of HCO_3^- and CO_3^{2-} ions that derived from limestone dissolution, resulting in lower pMC value.

All these observations and considerations suggest that the lamina-based dates should be corrected to match the pMC patterns with the atmospheric bomb peak (Fig. 8A). The raw lamina ages of NU-1 were shifted by 5 years relative to the

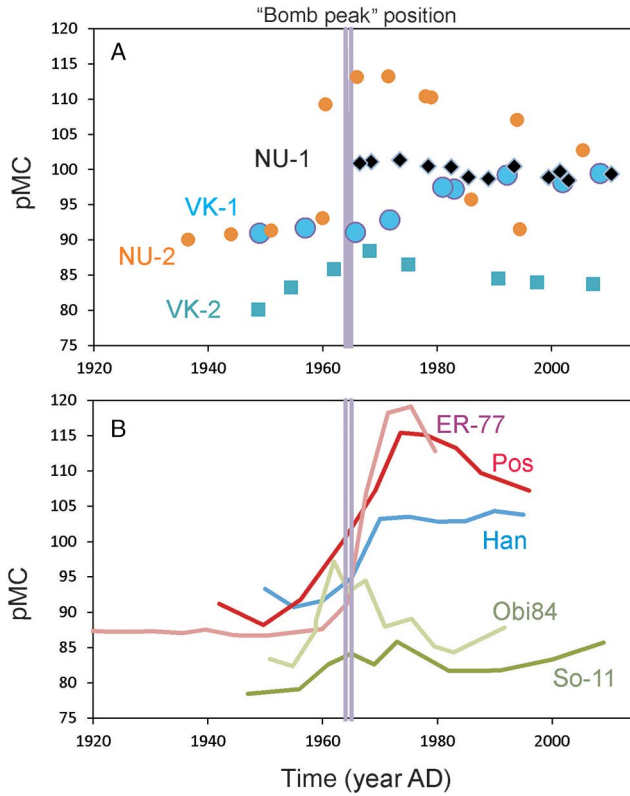


Fig. 6

A: Radiocarbon activity data (as pMC values) as a function of raw lamina counting dates calculated from the topmost laminae dated with collection dates and with no correction for possible hiatuses. B: Published radiocarbon activity data (as pMC values) as a function of time for European stalagmites. Data of ER-77, Pos, Han, Obi8, and So-11 are from Genty and Massault (1999) and Rudzka-Phillips et al. (2013)

collection date. A shift of 3 years was applied for the NU-2 stalagmite and an additional 5 years hiatus was placed before 1960 in order to achieve a realistic pattern. The raw lamina ages of VK-1 cannot be corrected using radiocarbon activity data alone, but a hiatus is apparent before 1970 (see later), while the ages for VK-2 were shifted by 5 years from the collection year of 2015. By this way, the isotope geochemical signal of each stalagmite could be uniformly synchronized to an established common timescale. In addition as the timescale of the atmospheric radiocarbon signal is the calendar timescale, it is a crucial prerequisite to compare the isotope geochemical signals to the meteorological parameters which are recorded on the same timescale, as shown later.

Plotting the ^{14}C activity data of the NU-1 stalagmite on a separate vertical axis (Fig. 8B), the internal variations can be better expressed that emphasized the

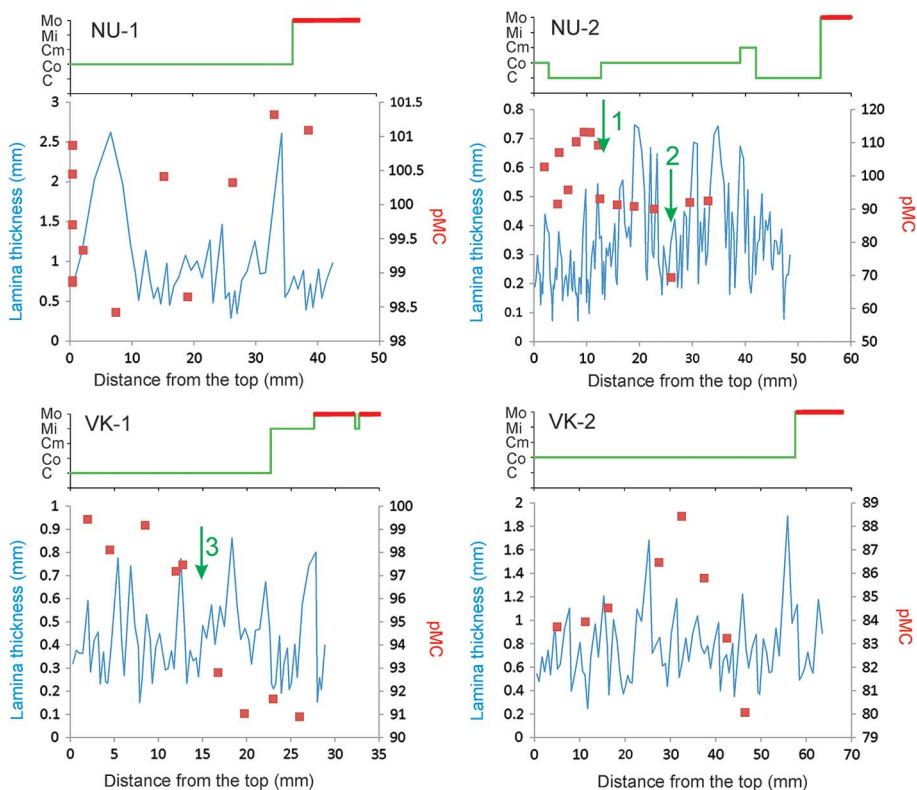


Fig. 7

Texture types (green and red lines), lamina thickness (in blue), and radiocarbon activity data (red squares) for the studied stalagmites. C: columnar. Co: open columnar. Cm: microcrystalline columnar. Mi: micritic. Mo: mosaic (following the terminology proposed by Frisia 2015). Stalagmite parts with mosaic texture are marked red due to their significance in alteration detection. Arrow 1: strong textural change in NU-2. Arrow 2: strong lamina thickness decrease associated with pMC drop. Arrow 3: position of disturbed texture in VK-1

appearance of the bomb peak in spite of the small variations in the stalagmite. The age corrections resulted not only in tuning of the bomb peaks, but also a systematic pattern can be detected in the ^{14}C activity data after about 1980. There are two periods (from ~1981 to ~1985 and from ~1992 to ~1999) when ^{14}C activities are low both in the NU-1 and the NU-2 stalagmites, which coherence in the activity patterns verifies the age-adjustment procedure.

The adjusted lamina counting dates were used to establish age–depth relationships for the individual stalagmites. The uncertainties of the age–depth relationships can be estimated by re-counting of the laminae and by fitting to anchoring dates. Re-counting

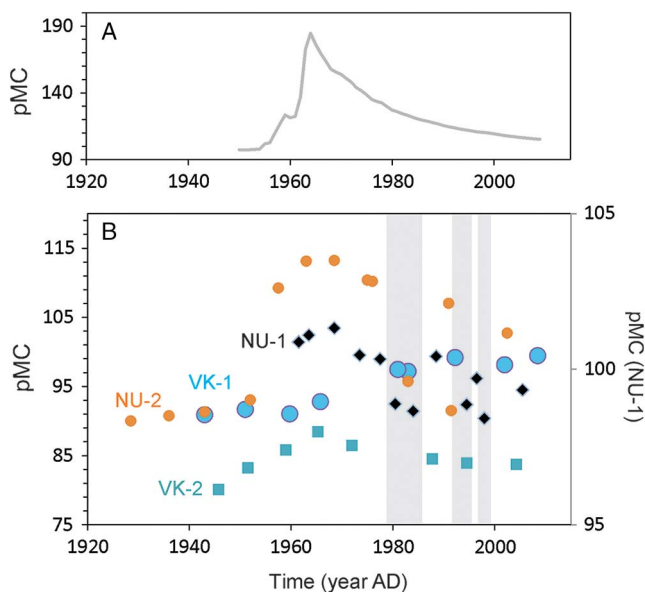


Fig. 8

A: Radiocarbon activity of atmospheric CO₂ in the spatially relevant NH1 zone (Hua et al. 2013). B: Radiocarbon activity data (as pMC values) as a function of lamina counting ages corrected for signal delay and possible hiatuses (see text). Note that the data of the NU-1 stalagmite are shown on separate vertical axis. Gray bars mark the periods of decreased pMC values in the NU stalagmites

the NU-1, NU-2, and VK-2 stalagmites' laminae resulted in differences of 2 years that can be regarded as a uncertainty of lamina counting. Since no fixed age dates are available, algorithms like the StalAge procedure (Scholz and Hoffmann 2011) could not be used. The positions of the ¹⁴C bomb peak (AD 1964) detected in the NU-2 and the VK-2 stalagmites are shown in Fig. 9, indicating a good match with the lamina counting.

An additional constraint is provided by the known date (1925) of construction work at the Vaskapu branch (Székely 2014). The ¹⁴C-based correction (see above) yields a deposition date of 1925 for the oldest detected lamina of the VK-2 stalagmite. Since lamina counting could not be conducted to the very base of the stalagmite, the model age of the beginning of the deposition can be some years earlier (between 1920 and 1925, compared with the known construction work in 1925). These observations collectively suggest that the uncertainty of the age–depth models is about 3–5 years. The porous stalagmites (NU-1 and VK-2) generally contain thicker laminae than the compact ones (NU-2 and VK-1), resulting in higher deposition rates (NU-1: 0.87 ± 0.06 mm year⁻¹ and VK-2: 0.73 ± 0.03 mm year⁻¹ compared with NU-2: 0.32 ± 0.01 mm year⁻¹ and VK-1: 0.37 ± 0.02 mm year⁻¹, Fig. 9).

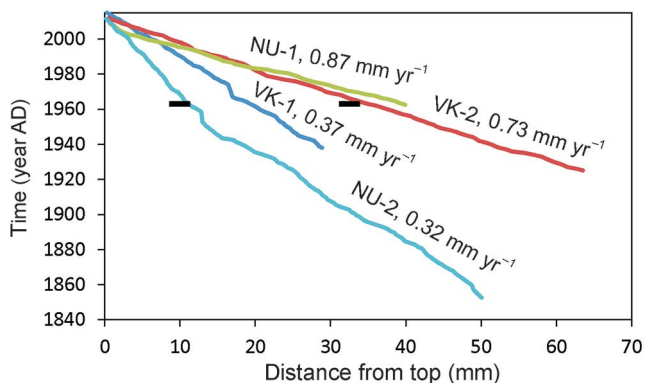


Fig. 9

Adjusted lamina counting dates (year AD) corrected for signal delay and hiatuses (see text) as a function of distance from the top for the studied stalagmites. Deposition rates are given as mm yr^{-1} . Black bars show the positions of ^{14}C bomb peak (AD 1963) for the NU-2 and VK-2 stalagmites

Stable C and O isotope compositions

As shown in Fig. 10, the studied stalagmites display systematic similarities and differences in their stable C and O isotope records. The NU-1 & VK-2 and the NU-2 & VK-1 pairs' similarities are best expressed in the $\delta^{13}\text{C}$ records. The NU-1 $\delta^{13}\text{C}$ values are perfectly replicated by the VK-2 stalagmite, whereas the $\delta^{13}\text{C}$ patterns are very similar for the VK-1 and the NU-2 records, but the $\delta^{13}\text{C}$ values are slightly shifted. As discussed above, the lamina age correction was not possible on the basis of ^{14}C activity data for the VK-1 stalagmite. In this case, the stable carbon isotope compositions were used for tuning the VK-1 record to the NU-2 data. No delay had to be applied to the lamina ages, but a 6-year-long hiatus was inserted before the lamina of 1972 (where a sharp textural change was detected) that resulted in a perfect match of the $\delta^{13}\text{C}$ records (Fig. 10A).

The $\delta^{18}\text{O}$ records show a more complex pattern (Fig. 10B). One of the most apparent deviations in the $\delta^{18}\text{O}$ records is the negative $\delta^{18}\text{O}$ shift observed for the oldest part of the NU-1 stalagmite. Since that part is composed of mosaic texture calcite that may indicate recrystallization (Frisia 2015) and hence alteration of the original geochemical composition, the $\delta^{18}\text{O}$ values of mosaic textured laminae of porous stalagmites (NU-1 and VK-2) were omitted. The $\delta^{13}\text{C}$ values of mosaic textured laminae show no deviations from the columnar parts, hence we can conclude that the recrystallization left the C isotope compositions intact. It is important to note that the isotope records of stalagmites with similar growth rates can be matched with each other (VK-1 with NU-2 and VK-2 with NU-1).

In order to make the stalagmite data comparable, the isotope records of the individual stalagmites were converted to anomalies from their mean values of the common overlapping period, resulting in values scattering around 0.

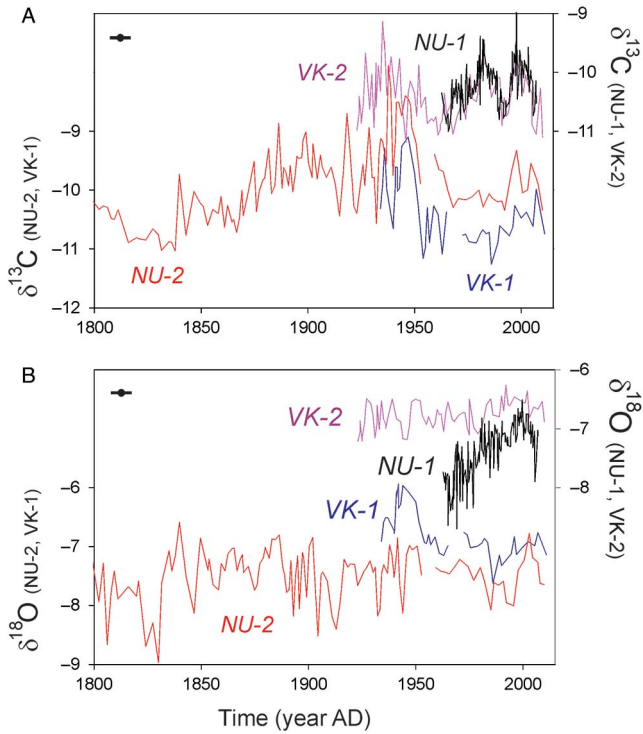


Fig. 10
 Stable C and O isotope compositions (in ‰ relative to V-PDB) of the studied stalagmites. The sample pairs of VK-1 & NU-2 and VK-2 & NU-1 are plotted in separate vertical axes, the scales are the same but they are shifted by 2‰ for more clear presentation. Black dot with horizontal bar shows 5 year uncertainty

$$\Delta^{13}\text{C}(i) = \delta^{13}\text{C}(i) - \delta^{13}\text{C}(\text{average}-i)$$

$$\Delta^{18}\text{O}(i) = \delta^{18}\text{O}(i) - \delta^{18}\text{O}(\text{average}-i),$$

where (i) denotes the stalagmite samples (NU-1, NU-2, VK-1, and VK-2), $\delta^{13}\text{C}(i)$ and $\delta^{18}\text{O}(i)$ are the measured isotope compositions, and $\delta^{13}\text{C}(\text{average}-i)$ and $\delta^{18}\text{O}(\text{average}-i)$ are the average compositions for the individual stalagmites.

The residual values are plotted as a function of corrected lamina ages in Fig. 11. The diagram shows compositions (marked by empty squares) that were obtained for stalagmites parts where mosaic texture appeared. The good fit of the paired records (see above) proves that the carbon isotopic compositions were not affected by the recrystallization processes (which resulted in the formation of mosaic texture). On the other hand, oxygen isotope compositions seem to be influenced, especially in the case of the NU-1 stalagmite. The $\delta^{18}\text{O}$ deviations between the otherwise similar NU-1 and VK-2 records caused by the strong negative $\delta^{18}\text{O}$ shift in the oldest part

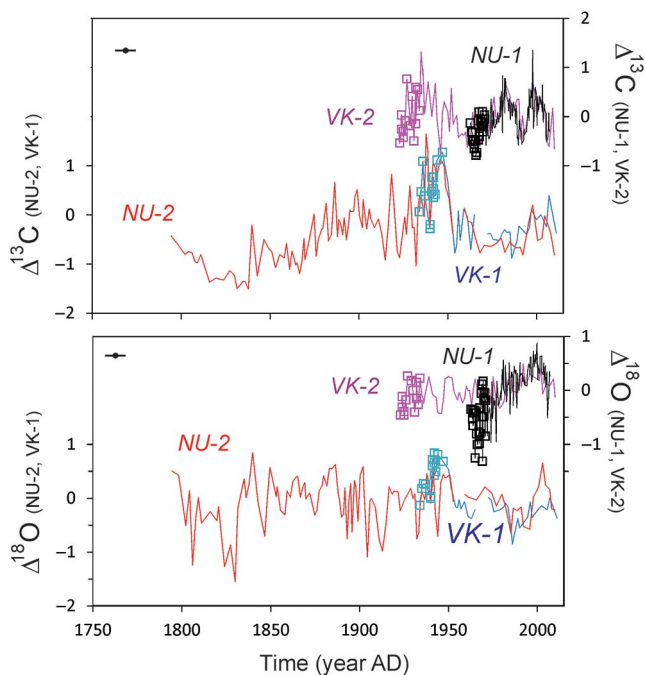


Fig. 11

Stable C and O isotope compositions expressed as anomalies from the average values of the individual stalagmites. Note that the sample pairs of VK-1 & NU-2 and VK-2 & NU-1 are plotted in separate Y axes, the scales are the same but they are shifted by 2‰ in order to avoid overlapping of the records. Empty squares mark the compositions obtained for laminae with mosaic texture. Black dot with horizontal bar shows 5 year uncertainty

of the NU-1 stalagmite suggests that the high porosity of the stalagmite resulted in enhanced sensitivity to late-stage re-equilibration. The isotopic similarities between the overlapping columnar and mosaic parts of the NU-2 and the VK-1 stalagmites indicate that the more compact fabric of these samples prevented them from the alteration.

In summary, the four stalagmites collected from two sites in nearby chambers of the same cave system form two pairs depending on the textural characteristics and growth rates. Slowly growing stalagmites (VK-1 and NU-2) are characterized by compact texture practically free of pores, whereas stalagmites (VK-2 and NU-1) with faster growth rates have very porous textures. The C and O isotope records show good correspondence within these pairs, hence composite records will be established for the two pairs. Isotope data for mosaic textured parts are omitted from the composite records, with the exception of the NU-2 stalagmite in which the mosaic textured layers also display a negative $\delta^{13}\text{C}$ peak, indicating that the $\delta^{18}\text{O}$ shift is at least partly related to primary, deposition-related processes.

Climate–composition relationships for fast-growing stalagmites

The composite $\delta^{13}\text{C}$ and $\delta^{18}\text{O}$ records for the NU-1 and VK-2 stalagmites were established by calculating annual average values (with missing years filled by averages of the preceding and following years) using both stalagmites' data. The $\delta^{18}\text{O}$ record does not contain those data that were obtained for mosaic textured calcite. As described in the Introduction section, stable carbon isotope compositions are mainly determined by soil activity related to humidity (precipitation amount), while the oxygen isotope composition of the precipitating carbonate is a result of competing effects of formation temperature and drip water composition (again affected by ambient temperature). Hence, the composite records were compared with gridded meteorological data (see Analytical methods section for details). The present evaluation is based only on a visual comparison of the isotopic and the meteorological records in order to determine the main factors that influence the isotopic compositions. Calculation of correlation coefficients can be misleading if coherency and secular variations are not evaluated. The correlation of two data sets can change within the entire period. Sub-periods can be characterized by opposite correlations and/or lead–lag relationships that can be quantified only by detailed evaluation (Wassenburg et al. 2016). A detailed statistical evaluation would exceed the limits of this study and will be the subject of a separate paper.

During the comparison of the composite $\delta^{13}\text{C}$ record with the CRU precipitation data, it was detected that the annual, the spring, and the summer averages of precipitation amount show no systematic relationships with the $\delta^{13}\text{C}$ values, while the winter and autumn precipitation amounts may have had appreciable influences (Fig. 12). The $\delta^{13}\text{C}$ values seem to show a long-term negative relationship with the winter precipitation, i.e., lower $\delta^{13}\text{C}$ values are generally associated with larger amount of winter precipitation. Larger amount of winter precipitation would result in improved soil humidity, enhanced biological activity in the vegetation seasons, and hence more biogenic carbon (with low $\delta^{13}\text{C}$ values) in the infiltrating drip water. This general scheme is in agreement with the observations. However, this relationship is modulated by autumn precipitation as most of the positive precipitation amount peaks correspond to elevated $\Delta^{13}\text{C}$ values. This unusual relationship can be explained by the dilution effect during rain events that flooded the open fractures and contributed to the annual infiltration.

The same procedure was followed for the comparison of the $\delta^{18}\text{O}$ and the CRU temperature records. In this case, only the autumn mean temperature showed weak positive relationships with the $\delta^{18}\text{O}$ record between 1946 and 2004 (Fig. 13). Warm peaks (shown by gray bars in Fig. 13) are generally associated with elevated $\delta^{18}\text{O}$ values, and the long-term rise in temperature between 1977 and 2004 appears also in almost continuous increase in the $\delta^{18}\text{O}$ record. After 2004 no relationship appears, whose reason is not known. The temperature variation in the cave is negligible in this time scale, hence the temperature variation can exert an effect by changing the meteoric water's – and hence the drip water's – composition. The local temperature

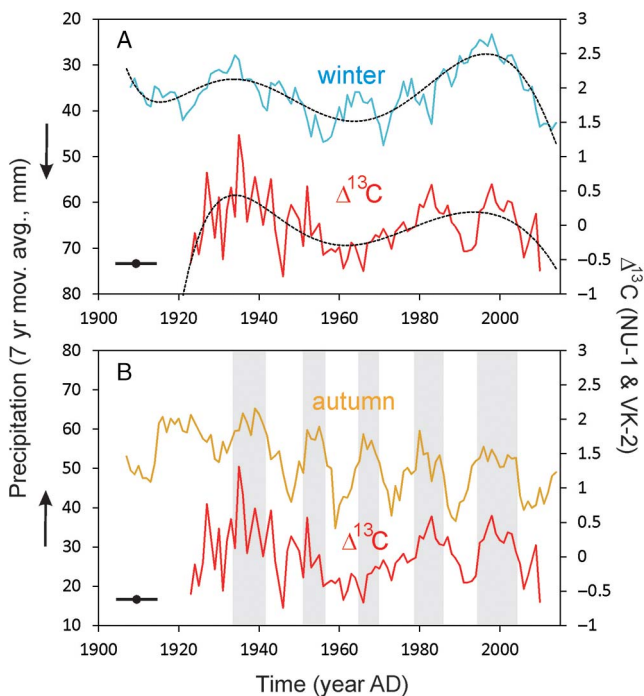


Fig. 12

Temporal variability of the composite carbon isotope record (expressed as deviation from the stalagmite $\delta^{13}\text{C}$ means, marked as $\Delta^{13}\text{C}$) for the VK-2 & NU-1 stalagmite pair and winter (A) and autumn (B) precipitation amounts (CRU TS3.23, Harris et al. 2014). Precipitation values are moving averages of the preceding 7 years. Note that the axes for precipitation amount are in different directions (as shown by the arrows). Dashed lines in (A) are sixth-order polynomial trends. Gray bars in (B) mark the periods of positive precipitation peaks. Black dot with horizontal bar shows 5 year uncertainty

$\delta^{18}\text{O}$ (water) gradient is about $0.3\text{‰}/\text{°C}$ (Czuppon, unpublished results, see Introduction section). The $\sim 1.5\text{ °C}$ variation would thus correspond to $\sim 0.5\text{‰}$ $\delta^{18}\text{O}$ change, close to the observed pattern. This observation indicates again that the fast-growing stalagmites are sensitive to rain events of autumn with a fast response to the changing dripping rate.

Climate–composition relationships for slowly growing stalagmites

The same procedure was applied for the establishment of the VK-1 & NU-2 composite isotope records as for the fast-growing stalagmite pair and the records were compared again with the CRU precipitation amount and temperature data (Figs 14 and 15). Although averages of the meteorological data of all the four seasons and annual means were compared with the isotope records, only the winter values showed

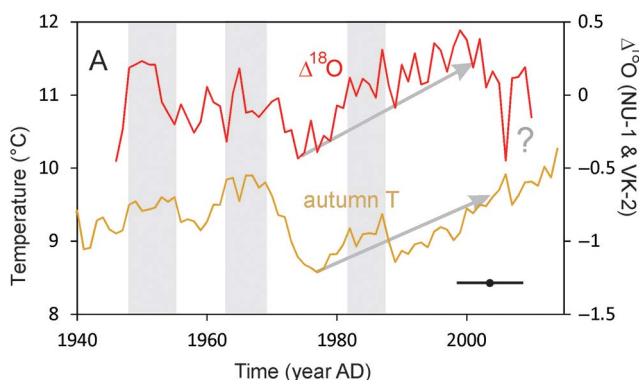


Fig. 13
 Composite oxygen isotope record (normalized to the stalagmite $\delta^{18}\text{O}$ means, marked as $\Delta^{18}\text{O}$) for the VK-2 & NU-1 stalagmite pair and autumn temperature (CRU TS3.23, Harris et al. 2014) as a function of age. Temperature values are moving averages of the preceding 7 years. Gray bars mark the periods of positive autumn temperature peaks, gray arrows show the period of rising temperature and $\delta^{18}\text{O}$ values. The question mark indicates the period of no relationship. Black dot with horizontal bar shows 5 year uncertainty

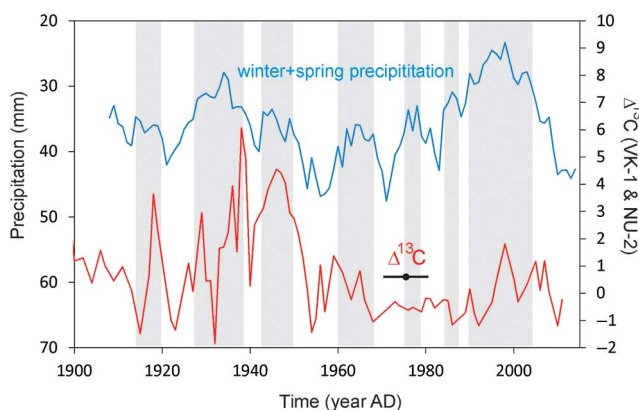


Fig. 14
 Composite carbon isotope record (normalized to the stalagmite $\delta^{13}\text{C}$ means, marked as $\Delta^{13}\text{C}$) for the VK-1 & NU-2 stalagmite pair and winter + spring (December to March) precipitation amounts (P) (CRU TS3.23; Harris et al. 2014) as a function of age. Precipitation values are moving averages of the preceding 7 years. Gray bars mark the periods of low P value peaks. Black dot with horizontal bar shows 5 year uncertainty

systematic relationships. Although the relationship is rather weak, higher $\delta^{13}\text{C}$ values tend to be associated with lower winter precipitation amount (marked by gray bars in Fig. 14), and higher $\delta^{18}\text{O}$ values generally correspond to higher winter temperatures (marked by gray bars in Fig. 15). These relationships are similar to those found for the

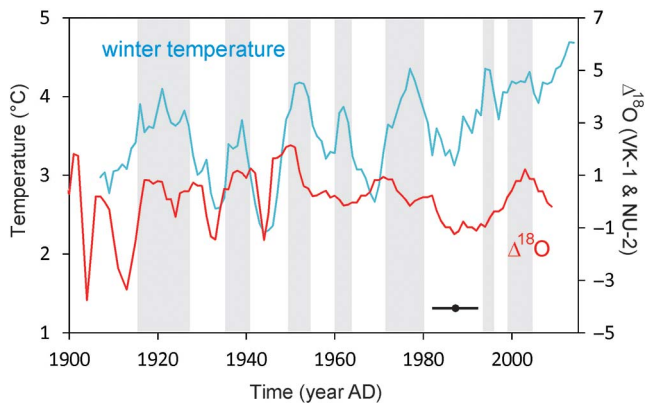


Fig. 15 Composite oxygen isotope record (normalized to the stalagmite $\delta^{18}\text{O}$ means, marked as $\Delta^{18}\text{O}$) for the VK-1 & NU-2 stalagmite pair and winter temperature (CRU TS3.23, Harris et al. 2014) as a function of age. Gray bars mark the periods of elevated temperature peaks. Black dot with horizontal bar shows 5 year uncertainty

fast-growing stalagmites, however pointing to a partially different infiltration season. Based on the long-term monthly precipitation/evapotranspiration data (Fig. 2), the main infiltration period at the site is winter and spring. The winter precipitation and temperature dependence of the isotope compositions of the slowly growing stalagmites is in agreement with this observation.

Trace element compositions as tracers of drip water origin and evolution

As we have seen, stable isotope compositions of fast and slowly growing stalagmites from nearby collection sites may reflect different seasonal precipitation and temperature signals, probably reflecting different infiltration pathways of the feeding drip water. These differences may also be expressed by trace element contents; especially Sr, Mg, Si, Al, and Th (see the comprehensive review of Fairchild and Baker 2012). The concentrations of Mg and Sr in the drip water and hence in the precipitating carbonate depends on many factors. Since these elements derive mainly from the host rock, the surrounding rocks' composition (e.g., the presence or absence of dolomitic layers) is the first factor. Longer residence time (slower water migration along the pathway) would result in elevated amounts of dissolved material and hence higher Sr and Mg concentrations in the stalagmite. Long residence time associated with ventilation in the fracture system can lead to carbonate precipitation, called prior calcite precipitation (PCP). PCP results in elevated Sr/Ca and Mg/Ca ratios due to the <1 K(Mg/Ca) and K(Sr/Ca) values (Tremaine and Froelich 2013; Borsato et al. 2016). Analyses of detrital elements like Si may help distinguish between limestone dissolution and PCP (Borsato et al. 2016). Once the drip water obtains its composition and the drops leave the caves ceiling, the trace element concentrations of the

stalagmite can be further modified by other factors. On the basis of experimental data, Huang and Fairchild (2001) proposed that Mg incorporation into the calcite is temperature-sensitive, while Sr incorporation depends on precipitation rate. Later studies have shown that paleohydrological variations causing changes in carbonate rock dissolution, solution concentration, or dilution and PCP can strongly modify or even determine the Mg and Sr contents of drip waters and the precipitating carbonate (Fairchild and Treble 2009; Fairchild and Baker 2012).

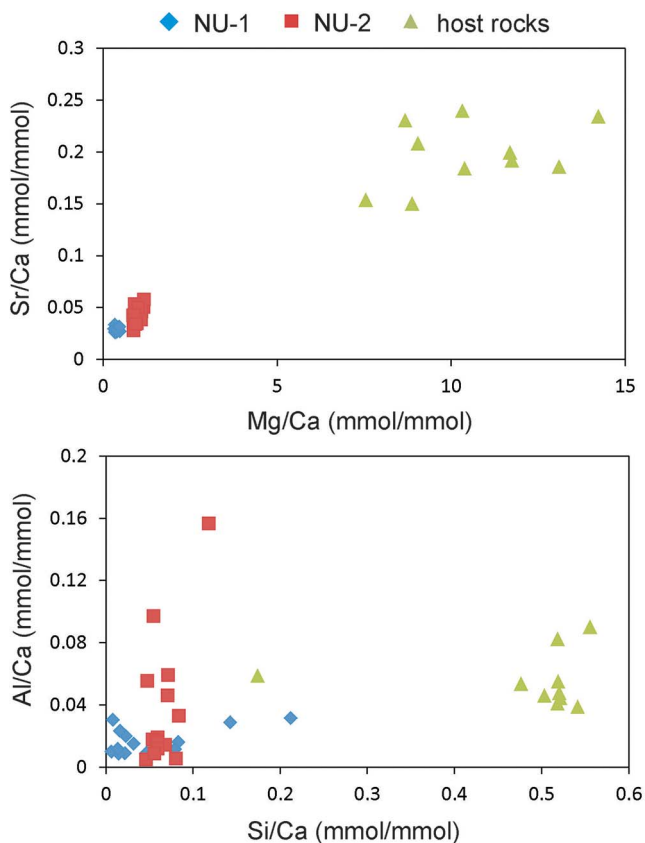
The concentrations of detrital elements may indicate further processes that affect the trace element concentrations. Dry periods lead to accumulation of detrital material on the stalagmite surface, reflected by high Si, Al, and Th contents (e.g., Fairchild and Baker 2012). Transient flushing of open fractures by rain events may carry detrital material and increase the precipitating carbonate's Si, Al, and Th contents, while the Sr and Mg concentrations may decrease due to dilution. These relationships suggest that combined evaluation of trace element compositions can shed light to the origin and evolution of drip waters.

Trace element compositions of two stalagmites of the Nehéz-út branch (NU-1 and NU-2) were determined in order to represent fast and slowly growing stalagmites, as well as their host rocks in the Baradla Cave. It is apparent that the NU-2 stalagmite has higher Sr and Mg concentrations relative to NU-1 and these compositions are shifted toward the host rocks' values (Fig. 16). PCP can result in such differences, but in that case the detrital component would not be different in the two cases. However, the Al/Ca and Si/Ca distributions (Fig. 16) have different slopes for the two stalagmites, indicating that they received detrital material from different sources, like soil-derived grains, wind-blown material, or dissolution residue produced by limestone dissolution. The most straightforward explanation for the difference in Al/Ca and Si/Ca distribution is that the stalagmites received drip water from different migration pathways. The slightly elevated Sr and Mg contents in the NU-2 stalagmite relative to the NU-1 sample indicate slower migration and longer residence time, resulting in more effective limestone dissolution.

Conclusions: Synthesis of drip water migration pathways and stalagmite formation environments

The main observations obtained in this study are the following:

- (1) Four actively forming stalagmites (NU-1, NU-2, VK-1, and VK-2) were collected from two sites (Nehéz-út and Vaskapu) close to each other. The stalagmites can be divided into two pairs by macroscopic appearance and textural characteristics. Two stalagmites (NU-1 and VK-2) showed irregular forms and very porous inner fabric, while the other two (NU-2 and VK-1) are characterized by isometric forms and dense and compact internal fabric. The stalagmites are composed of calcite with different textural types (columnar, micritic, and mosaic).



- (4) Raw lamina counting dates were corrected for delays and hiatuses on the basis of textural observations and radiocarbon activity patterns, then the adjusted dates were used to establish age–depth models for the individual stalagmites. By this way, the isotope geochemical signal of each stalagmite could be uniformly synchronized to an established timescale. Porous stalagmites were found to have formed at higher deposition rates than those with compact textures.
- (5) Stable C and O isotope compositions were measured and compared for the four stalagmites at high resolution (~0.5 mm, corresponding to <1 to ~5 years). The isotope records of stalagmites with similar growth rates fit well each other, but there are significant differences between fast and slowly growing stalagmite pairs. The C and O isotope compositions were also compared with meteorological data that revealed that the fast-growing stalagmites are sensitive mainly to winter and autumn precipitation and temperature, hence their formation may be affected by transient rain events. The slowly growing stalagmites are sensitive to winter precipitation and temperature, hence their formation is determined by the main infiltration period.
- (6) Interpretations of trace element (Sr, Mg, Al, and Si) concentrations also supported that the fast/slow depositing stalagmite pairs were formed from drip waters originating from different infiltration regimes.

All these pieces of information can be synthesized in a model (Fig. 17). The drip water feeding the fast-growing (NU-1 and VK-2) stalagmites may have infiltrated in a doline with thick soil cover and migrated in open fractures. The larger amount of old organic matter in the soil contributed with low ^{14}C activity carbon that decreased the overall pMC values and smoothed the bomb peak. The water collection in the doline and the fast throughput in the fracture system made the stalagmites sensitive to transient rain events. The shorter residence time lead to less effective limestone dissolution and lower Sr and Mg contents in the drip water and in the stalagmites.

On the contrary, the slowly growing stalagmites may have received drip water from a diffuse fracture system developed below thin soil cover. The lack of significant amount of old organic matter resulted in elevated ^{14}C activities and a well-developed bomb peak in NU-2. The diffuse fracture system and the slow water migration lead to more effective limestone dissolution, and hence higher Sr and Mg concentrations in the drip water and in the stalagmites. As a further consequence, the system is more sensitive to the snow melting and the main infiltration period, i.e., winter precipitation and temperature determine the isotopic compositions. The very close positions of fast and slowly growing stalagmites with different geochemical signatures indicate horizontal water migration beside the vertical fracture system.

Since the slowly growing stalagmites are less prone to late-stage alterations and less sensitive to transient rain events, their composite $\delta^{13}\text{C}$ and $\delta^{18}\text{O}$ records are selected for further statistical analyses and comparison with meteorological data and stalagmite records of the region.

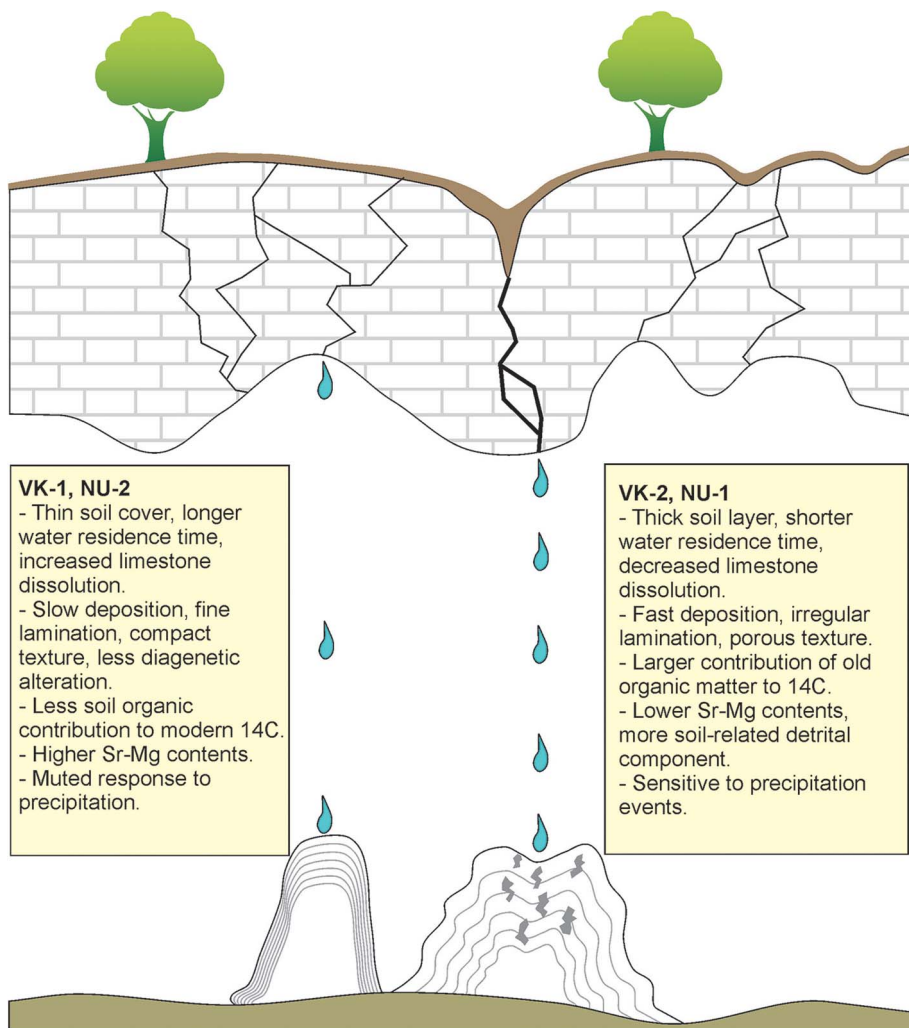


Fig. 17
Model scheme of different drip water infiltration pathways and their effects on stalagmite composition

Acknowledgements

Constructive and helpful reviews by Anamaria Häuselmann and Yuri Dublyanski greatly helped to improve the paper and clarify our ideas, and are gratefully acknowledged. The authors also thank Silvia Frisia who kindly helped with the interpretation of textural features. This research was supported by the Hungarian

Scientific Research Fund (OTKA NK 101664). The János Bolyai Research Scholarship of the Hungarian Academy of Sciences financially supported GC's work. This is contribution no. 40 of the 2ka Palaeoclimatology Research Group.

References

- Baker, A., A. Asrat, I.J. Fairchild, M.J. Leng, P.M. Wynn, C. Bryant, D. Genty, M. Umer 2007: Analysis of the climate signal contained within $\delta^{18}\text{O}$ and growth rate parameters in two Ethiopian stalagmites. – *Geochimica et Cosmochimica Acta*, 71, pp. 2975–2988.
- Baker, A., C.L. Smith, C. Jex, I.J. Fairchild, D. Genty, L. Fuller 2008: Annually laminated speleothems: A review. – *International Journal of Speleology*, 37, pp. 193–206.
- Baker, A.J., D.P. Matthey, J.U.L. Baldini 2014: Reconstructing modern stalagmite growth from cave monitoring, local meteorology, and experimental measurements of dripwater films. – *Earth and Planetary Science Letters*, 392, pp. 239–249.
- Bartholy, J., R. Pongrácz, M. Pattantyús-Ábrahám 2006: European cyclone track analysis based on ECMWF ERA-40 data sets. – *International Journal of Climatology*, 26, pp. 1517–1527.
- Bartholy, J., R. Pongrácz, M. Pattantyús-Ábrahám 2009: Analyzing the genesis, intensity, and tracks of western Mediterranean cyclones. – *Theoretical and Applied Climatology*, 96, pp. 133–144.
- Boch, R., C. Spötl 2011: Reconstructing palaeoprecipitation from an active cave flowstone. – *Journal of Quaternary Science*, 26, pp. 675–687.
- Boch, R., C. Spötl, S. Frisia 2011: Origin and palaeoenvironmental significance of lamination in stalagmites from Katerloch Cave, Austria. – *Sedimentology*, 58, pp. 508–531.
- Borsato, A., V.E. Johnston, S. Frisia, R. Miorandi, F. Corradini 2016: Temperature and altitudinal influence on Karst dripwater chemistry: Implications for regional-scale palaeoclimate reconstructions from Speleothems. – *Geochimica et Cosmochimica Acta*, 177, pp. 275–297.
- Bottyán, E., Gy. Czuppon, T. Weidinger, L. Haszpra, K. Kármán 2013: Determination of air moisture source region for precipitation in Hungary. – *Central European Geology*, 56, p. 273.
- Casteel, R.C., J.L. Banner 2015: Temperature-driven seasonal calcite growth and drip water trace element variations in a well-ventilated Texas cave: Implications for speleothem paleoclimate studies. – *Chemical Geology*, 392, pp. 43–58.
- Curl, R.L. 1973: Minimum diameter stalagmites. – *Bulletin of the National Speleological Society*, 35, pp. 1–9.
- Czuppon, G., E. Bottyán, T. Weidinger, K. Kármán, L. Haszpra 2015: Spatial and temporal variabilities in stable isotope compositions of precipitation and air moisture sources in Hungary. – In: *International Symposium on Isotope Hydrology: Revisiting Foundations and Exploring Frontiers*, IAEA, p. 57.
- Czuppon, Gy., A. Demény, Sz. Leél-Óssy, M. Óvári, M. Molnár, J. Stieber, K. Kármán, K. Kiss, L. Haszpra submitted: Cave monitoring in Béke and Baradla Caves (NE Hungary): Implications for the condition of the formation of cave carbonates. – *Quaternary International* (under review).
- Dansgaard, W. 1964: Stable isotopes in precipitation. – *Tellus*, 16/4, pp. 436–468.
- Demény, A., Gy. Czuppon, Z. Kern, Sz. Leél-Óssy, A. Németh, M. Szabó, M. Tóth, Ch. Wu, Ch. Shen, M. Molnár, T. Németh, P. Németh, M. Óvári 2016: Recrystallization-induced oxygen isotope changes in inclusion-hosted water of speleothems – Paleoclimatological implications. – *Quaternary International*, 415, pp. 25–32.
- Dietzel, M., J. Tang, A. Leis, S.J. Köhler 2009: Oxygen isotopic fractionation during inorganic calcite precipitation – Effects of temperature, precipitation rate and pH. – *Chemical Geology*, 268, pp. 107–115.
- Dorale, J.A., Z. Liu 2009: Limitations of Hندی test criteria in judging the paleoclimatic suitability of speleothems and the need for replication. – *Journal of Cave and Karst Studies*, 71, pp. 73–80.

- Duan, W., J. Ruan, W. Luo, T. Li, L. Tian, G. Zeng, D. Zhang, Y. Bai, J. Li, T. Tao, P. Zhang, A. Baker, M. Tan 2016: The transfer of seasonal isotopic variability between precipitation and drip water at eight caves in the monsoon regions of China. – *Geochimica et Cosmochimica Acta*, 183, pp. 250–266.
- Fairchild, I.J., P.C. Treble 2009: Trace elements in speleothems as recorders of environmental change. – *Quaternary Science Reviews*, 28, pp. 449–468.
- Fairchild, I.J., A. Baker 2012: *Speleothem Science*. – Wiley-Blackwell, 450 p.
- Fórizs, I. 2003: Isotopes as natural tracers in the water cycle: Examples from the Carpathian Basin. – *Studia Universitatis Babeş-Bolyai, Physica, Special Issue XLVIII*, pp. 69–77.
- Frisia, S. 2015: Microstratigraphic logging of calcite fabrics in speleothems as tool for palaeoclimate studies. – *International Journal of Speleology*, 44, pp. 1–16.
- Frisia, S., A. Borsato, I.J. Fairchild, F. McDermott 2000: Calcite fabrics, growth mechanisms and environments of formation in speleothems from the Italian Alps and southwestern Ireland. – *Journal of Sedimentary Research*, 70, pp. 1183–1196.
- Frisia, S., A. Borsato, R. Drysdale, B. Paul, A. Greig, M. Cotte 2012: A re-evaluation of the palaeoclimatic significance of phosphorus variability in speleothems revealed by high-resolution synchrotron micro XRF mapping. – *Climate of the Past*, 8, pp. 2039–2051.
- Genty, D. 2008: Palaeoclimate research in Villars Cave (Dordogne, SW-France). – *International Journal of Speleology*, 37, pp. 173–191.
- Genty, D., M. Massault 1999: Carbon transfer dynamics from bomb-¹⁴C and δ^{13} C time series of a laminated stalagmite from SW France – Modelling and comparison with other stalagmite records. – *Geochimica et Cosmochimica Acta*, 63, pp. 1537–1548.
- Genty, D., A. Baker, W. Barnes 1997: Comparaison entre les lamines luminescentes et les lamines visibles annuelles de stalagmites (Comparison of annual luminescent and visible laminae in stalagmites). – *Comptes Rendus de l'Académie des Sciences – Series IIA – Earth and Planetary Science*, 325, pp. 193–200.
- Harris, I., P.D. Jones, T.J. Osborn, D.H. Lister 2014: Updated high-resolution grids of monthly climatic observations – The CRU TS3.10 Dataset. – *International Journal of Climatology*, 34, pp. 623–642.
- Hendy, C.H. 1971: The isotopic geochemistry of speleothems: 1. The calculation of the effects of the different modes of formation on the isotopic composition of speleothems and their applicability as palaeoclimatic indicators. – *Geochimica et Cosmochimica Acta*, 35, pp. 801–824.
- Holko, L., M. Dóša, J. Michalko, M. Šanda 2012: Isotopes of oxygen-18 and deuterium in precipitation in Slovakia. – *Journal of Hydrology and Hydromechanics*, 60, pp. 265–276.
- Hua, Q., M. Barbetti, A.Z. Rakowski 2013: Atmospheric radiocarbon for the period 1950–2010. – *Radiocarbon*, 55, pp. 2059–2072.
- Huang, Y., I.J. Fairchild 2001: Partitioning of Sr²⁺ and Mg²⁺ into calcite under Karst-analogue experimental conditions. – *Geochimica et Cosmochimica Acta*, 65, pp. 47–62.
- Kelemen, F.D., J. Bartholy, R. Pongrácz 2015: Multivariable cyclone analysis in the Mediterranean region. – *Időjárás*, 119/2, pp. 159–184.
- Lachniet, M.S. 2009: Climatic and environmental controls on speleothem oxygen-isotope values. *Quaternary Science Reviews*, 28, pp. 412–432.
- Mattey, D., D. Lowry, J. Duffet, R. Fisher, E. Hodge, S. Frisia 2008: A 53 year seasonally resolved oxygen and carbon isotope record from a modern Gibraltar speleothem: Reconstructed drip water and relationship to local precipitation. – *Earth and Planetary Science Letters*, 269, pp. 80–95.
- Mattey, D.P., T.C. Atkinson, J.A. Barker, R. Fisher, J.P. Latin, R. Durrell, M. Ainsworth 2016: Carbon dioxide, ground air and carbon cycling in Gibraltar Karst. – *Geochimica et Cosmochimica Acta*, 184, pp. 88–113.
- McDermott, F., S. Frisia, Y. Huang, A. Longinelli, B. Spiro, T.H.E. Heaton, C.J. Hawkesworth, A. Borsato, E. Keppens, I.J. Fairchild, K. van der Borg, S. Verheyden, E. Selmo 1999: Holocene climate variability in Europe: Evidence from δ^{18} O and textural variations in speleothems. – *Quaternary Science Reviews*, 18, pp. 1021–1038.

- Meyer, K.W., W. Feng, D.O. Breecker, J.L. Banner, A. Guilfoyle 2014: Interpretation of speleothem calcite $\delta^{13}\text{C}$ variations: Evidence from monitoring soil CO_2 , drip water, and modern speleothem calcite in central Texas. – *Geochimica et Cosmochimica Acta*, 142, pp. 281–298.
- Mickler, P.J., L.A. Stern, J.L. Banner 2006: Large kinetic isotope effects in modern speleothems. – *GSA Bulletin*, 118, pp. 65–81.
- Mischel, S.A., D. Scholz, C. Spötl 2015: $\delta^{18}\text{O}$ values of cave drip water: A promising proxy for the reconstruction of the North Atlantic Oscillation? – *Climate Dynamics*, 45, pp. 3035–3050.
- Molnár, M., R. Janovics, I. Major, J. Orsovski, R. Gönczi, M. Veres, A.G. Leonard, S.M. Castle, T.E. Lange, L. Wacker, I. Hajdas, A.J.T. Jull 2013a: Status report of the new AMS C-14 sample preparation lab of the Hertelendi Laboratory of Environmental Studies, Debrecen, Hungary. – *Radiocarbon*, 55/2–3, pp. 665–676.
- Molnár, M., L. Rinyu, M. Veres, M. Seiler, L. Wacker, H.A. Synal 2013b: EnvironMICADAS: A mini 14C-AMS with enhanced gas ion source interface in the Hertelendi Laboratory of Environmental Studies (HEKAL), Hungary. – *Radiocarbon*, 55/2–3, pp. 338–344.
- Moquet, J.S., F.W. Cruz, V.F. Novello, N.M. Strikis, M. Deininger, I. Karmann, R. Ventura Santos, C. Millo, J. Apaestegui, J.L. Guyot, A. Siffedine, M. Vuille, H. Cheng, R.L. Edwards, W. Santini 2016: Calibration of speleothem $\delta^{18}\text{O}$ records against hydroclimate instrumental records in Central Brazil. – *Global and Planetary Change*, 139, pp. 151–164.
- Moreno, A., C. Sancho, M. Bartolomé, B. Oliva-Urcia, A. Delgado-Huertas, M.J. Estrela, D. Corell, J.I. López-Moreno, I. Cacho 2014: Climate controls on rainfall isotopes and their effects on cave drip water and speleothem growth: The case of Molinos cave (Teruel, NE Spain). – *Climate Dynamics*, 43, pp. 221–241.
- Muñoz-García, M.B., J. Cruz, J. Martín-Chivelet, A.I. Ortega, M.J. Turrero, M. Lopez-Elorza 2016: Comparison of speleothem fabrics and microstratigraphic stacking patterns in calcite stalagmites as indicators of paleoenvironmental change. – *Quaternary International*, 407, pp. 74–85.
- O’Neil, J.R., R. Clayton, T. Mayeda 1969: Oxygen isotopic fractionation in divalent metal carbonates. – *The Journal of Chemical Physics*, 51, pp. 5547–5558.
- Orland, I.J., Y. Burstyn, M. Bar-Matthews, R. Kozdon, A. Ayalon, A. Matthews, J.W. Valley 2014: Seasonal climate signals (1990–2008) in a modern Soreq Cave stalagmite as revealed by high-resolution geochemical analysis. – *Chemical Geology*, 363, pp. 322–333.
- Osácar, M.C., C. Sancho, A. Muñoz, M. Bartolomé, A. Moreno, A. Delgado-Huertas, I. Cacho 2014: Tracking the oxygen isotopic signature from the rainfall to the speleothems in Ortigosa de Cameros caves (La Rioja, Spain). – *Estudios Geológicos*, 70/2, p. e021.
- Pu, J., A. Wang, J. Yin, L. Shen, Y. Sun, D. Yuan, H. Zhao 2015: Processes controlling dripwater hydrochemistry variations in Xueyu Cave, SW China: Implications for speleothem palaeoclimate signal interpretations. – *Boreas*, 44/3, pp. 603–617.
- Pu, J., A. Wang, L. Shen, J. Yin, D. Yuan, H. Zhao 2016: Factors controlling the growth rate, carbon and oxygen isotope variation in modern calcite precipitation in a subtropical cave, Southwest China. – *Journal of Asian Earth Sciences*, 119, pp. 167–178.
- Riechelmann, D.F.C., A. Schröder-Ritzrau, D. Scholz, J. Fohlmeister, C. Spötl, D.K. Richter, A. Mangini 2011: Monitoring Bunker Cave (NW Germany): A prerequisite to interpret geochemical proxy data of speleothems from this site. – *Journal of Hydrology*, 409, pp. 682–695.
- Rozanski, K., L. Araguas-Araguas, R. Gonfiantini 1993: Isotopic Patterns in Modern Global Precipitation. *Climate Change in Continental Isotopic Records*. – American Geophysical Union, Geophysical Monograph, 78, pp. 1–36.
- Rudzka-Phillips, D., F. McDermott, A. Jackson, D. Fleitmann 2013: Inverse modelling of the ^{14}C bomb pulse in stalagmites to constrain the dynamics of soil carbon cycling at selected European cave sites. – *Geochimica et Cosmochimica Acta*, 112, pp. 32–51.
- Salamalikis, V., V.V. Argiriou, E. Dotsika 2016: Periodicity analysis of $\delta^{18}\text{O}$ in precipitation over Central Europe: Time–frequency considerations of the isotopic ‘temperature’ effect. – *Journal of Hydrology*, 534, pp. 150–163.

- Scholz, D., D.L. Hoffmann 2011: StalAge – An algorithm especially designed for construction of speleothem age. – *Quaternary Geochronology*, 6, pp. 369–382.
- Scholz, D., C. Mühlinghaus, A. Mangini 2009: Modelling $\delta^{13}\text{C}$ and $\delta^{18}\text{O}$ in the solution layer on stalagmite surfaces. – *Geochimica et Cosmochimica Acta*, 73, pp. 2592–2602.
- Spötl, C., T.W. Vennemann 2003: Continuous-flow IRMS analysis of carbonate minerals. – *Rapid Communications in Mass Spectrometry*, 17, pp. 1004–1006.
- Szalai, S., I. Auer, J. Hiebl, J. Milkovich, T. Radim, P. Štěpánek, P. Zahradníček, Z. Bihari, M. Lakatos, T. Szentimrey, D. Limanowka, P. Kilar, S. Cheval, Gy. Deák, D. Mihić, I. Antolović, V. Mihajlović, P. Nejedlik, P. Stastny, K. Mikulova, I. Nabyvanets, O. Skyryk, S. Krakovskaya, J. Vogt, T. Antofie, J. Spinoni 2013: Climate of the greater Carpathian region. Final Technical Report. – www.carpatlim-eu.org.
- Székely, K. 2014: A Baradla története (The history of Baradla). – In: Gruber, P., L. Gaál (Eds): A Baradla–Domica barlangrendszer (The Baradla–Domica Cave System). Aggtelek National Park, pp. 367–420. (in Hungarian)
- Treble, P.C., I.J. Fairchild, A. Griffiths, A. Baker, K.T. Meredith, A. Wood, E. McGuire 2015: Impacts of cave air ventilation and in-cave prior calcite precipitation on Golgotha Cave dripwater chemistry, southwest Australia. – *Quaternary Science Reviews*, 127, pp. 61–72.
- Tremaine, D.M., P.N. Froelich 2013: Speleothem trace element signatures: A hydrologic geochemical study of modern cave dripwaters and farmed calcite. – *Geochimica et Cosmochimica Acta*, 121, pp. 522–545.
- Van Rampelbergh, M., S. Verheyden, M. Allan, Y. Quinif, E. Keppens, P. Claeys 2014: Monitoring of a fast-growing speleothem site from the Han-sur-Lesse cave, Belgium, indicates equilibrium deposition of the seasonal $\delta^{18}\text{O}$ and $\delta^{13}\text{C}$ signals in the calcite. – *Climate of the Past*, 10, pp. 1871–1885.
- Van Rampelbergh, M., S. Verheyden, M. Allan, Y. Quinif, H. Cheng, L.R. Edwards, E. Keppens, P. Claeys 2015: A 500-year seasonally resolved $\delta^{18}\text{O}$ and $\delta^{13}\text{C}$, layer thickness and calcite aspect record from a speleothem deposited in the Han-sur-Lesse cave, Belgium. – *Climate of the Past*, 11, pp. 789–802.
- Vodila, G., L. Palcsu, I. Futó, Zs. Szántó 2011: A 9-year record of stable isotope ratios of precipitation in Eastern Hungary: Implications on isotope hydrology and regional palaeoclimatology. – *Journal of Hydrology*, 400, pp. 144–153.
- Wassenburg, J.A., S. Dietrich, J. Fietzke, J. Fohlmeister, K.P. Jochum, D. Scholz, D.K. Richter, A. Sabaoui, C. Spötl, G. Lohmann, M.O. Andrae, A. Immenhauser 2016: Reorganization of the North Atlantic Oscillation during early Holocene deglaciation. – *Nature Geoscience*, 9, pp. 602–605.